UC Irvine

UC Irvine Electronic Theses and Dissertations

Title

A visual field map of perceptual confidence

Permalink

https://escholarship.org/uc/item/00w95950

ISBN

9798177368085

Author

Shen, Angela

Publication Date

2026-11-26

Copyright Information

This work is made available under the terms of a Creative Commons Attribution-NonCommercial-NoDerivatives License, available at https://creativecommons.org/licenses/by-nc-nd/4.0/

Peer reviewed|Thesis/dissertation

eScholarship.org Powered by the California Digital Library
University of California

UNIVERSITY OF CALIFORNIA,

IRVINE

A visual field map of perceptual confidence

DISSERTATION

submitted in partial satisfaction of the requirements

for the degree of

DOCTOR OF PHILOSOPHY

in Cognitive Sciences

by

Angela Shen

Dissertation Committee:

Professor Megan Peters, Chair

Professor Barbara Dosher

Professor Mark Steyvers

2026

© 2026 Angela Shen

To my brilliant ah-po (grandma), 许焕英,

who took me to the library every week when I was too young to understand that education is a privilege, but not a luxury.

"The inner machinations of my mind are an enigma."

—Patrick Star

CONTENTS

Acknowledgments **vii**

Vita **viii**

Abstract **x**

General Introduction **1**

1 Stable metacognition across an asymmetric visual field **6**

1.1 Abstract 6

1.2 Introduction 7

1.3 Results 8

1.3.1 Experimental task 8

1.3.2 Visual field asymmetries persist in objective performance 9

1.3.3 The relationship between confidence and performance shows little evidence of systematic visual field asymmetries 10

1.3.4 Metacognitive sensitivity is relatively stable across the visual field after accounting for perceptual performance 11

1.4 Discussion 12

1.5 Methods 14

1.5.1 Observers 14

1.5.2 Apparatus 14

1.5.3 Main task 15

1.5.4 Thresholding 17

1.5.5 Data analysis 18

1.5.6 Statistical analysis 21

2 Stimulus properties and visual field location interact to drive performance-independent perceptual confidence **23**

2.1 Abstract . . . 23

2.2 Introduction . . . 24

2.3 Experiment 1 . . . 27

2.3.1 Methods . . . 27

2.3.2 Results . . . 33

2.4 Experiment 2 . . . 36

2.4.1 Methods . . . 36

2.4.2 Results . . . 37

2.5 Discussion . . . 38

2.6 Appendix . . . 45

3 The geometry of perceptual confidence **51**

3.1 Abstract . . . 51

3.2 Introduction . . . 52

3.3 Methods . . . 55

3.3.1 Data preprocessing and construction of accuracy-speed trajectories . . . 55

3.3.2 Modeling confidence as a joint function of accuracy and response speed . . . 56

3.3.3 Construction of the empirical confidence surface . . . 59

3.3.4 Eccentricity-specific confidence surfaces and nVUS . . . 62

3.3.5 Polar angle-specific confidence surfaces and nVUS . . . 62

3.3.6 Statistical analysis . . . 63

3.4 Results . . . 63

3.4.1 Preprocessing results . . . 63

3.4.2 Confidence as a joint function of accuracy and response speed . . . 63

3.4.3 Confidence surfaces across eccentricity . . . 66

3.4.4 Confidence surfaces across polar angle . . . 67

3.5 Discussion . . . 69

3.5.1 Limitations and future directions . . . 71

3.5.2 Conclusion 72

General Conclusion **74**

List of Figures

1.1 Contrast thresholds and visual field asymmetries. 9

1.2 Confidence for matched performance range across the visual field. 10

1.3 Trial sequence and stimuli. 17

2.1 Stimuli & trial sequence. 30

2.2 Experiment 1 results. 35

2.3 Experiment 2 results. 39

3.1 Reaction time as a function of stimulus contrast and visual field location. 54

3.2 Joint distribution of accuracy and response speed. 58

3.3 Observer-level accuracy-speed trajectories across visual field locations. 60

3.4 Observer-level empirical support in accuracy-speed space. 61

3.5 Model-predicted confidence as a function of accuracy and response speed across visual field locations. 64

3.6 Predicted confidence as a joint function of accuracy and response speed across eccentricities. 66

3.7 Normalized volume under the surface (nVUS) across eccentricity. 67

3.8 Predicted confidence as a joint function of accuracy and response speed across polar angles. 68

3.9 Normalized volume under the surface (nVUS) across polar angle. 69

ACKNOWLEDGMENTS

Megan Peters does, in fact, have the solutions to every problem, including to *how to be the best mentor*.

Brian Maniscalco has been called the three-eyed raven.

Barbara Dosher and Mark Steyvers are likely the only ones who will read this. Hello! Thank you!

How many collaborators does it take to power the light bulb above my head? At least 4: Jorge Morales, Rachel Denison, Karen Tian, and Xueyi Huang.

Brian Odegaard is adored by mentees and manatees.

Michael Lee is an excellent guitar student (I've heard) and guitar player (I haven't heard).

Jeff Rouder once made me watch the penultimate scene from *Moneyball*.

Mathieu Landry, Amir Raz, Daina Crafa, and Marisa Carrasco thought I could do better.

Nina Hanning bestowed upon me the formula to sow (scientific) chaos. Michael Jigo is about as great as a Dough donut. Antonio Fernández went out one night to stargaze and accidentally ate Polaris — he's all we've got now.

Tracy Chen and Kiarra Michelle Garcia see me happily waving in their rearview mirrors.

To everyone who was generous enough to participate in my 8-hour studies: You're the only ones without whom this work would not be possible.

Allison Morehouse and I are growing up in science.

Talía Román is absolutely worth traveling the distance for.

Helen Braithwaite witnessed the moon landing of this generation.

Jacky Beck is my day one.

Manuel Villarreal is my best friend once removed.

Mahbod Mehrvarz must be gleefully acknowledged.

For 40 days a year, Lauren Montgomery chooses me over gummy candies or Reddit.

Shaida Abachi is a rare snow leopard.

Ruby Greenberg and I can now resume coven activities.

Daniel Durst has made fools of you all.

Prawit Siriwat is all of the universe's very best things distilled in one uneasy container.

++ big hugs to Chompers and Zazzles. We're going home!

I would like to acknowledge the support of the Natural Sciences and Engineering Council of Canada (NSERC) through a Postgraduate Scholarship-Doctoral award (PGSD3-557914-2021).

VITA

ANGELA SHEN

2026	Ph.D. in Cognitive Sciences, University of California, Irvine
2024	M.S. in Cognitive Sciences, University of California, Irvine
2020	M.A. in Psychology, New York University
2017	B.A. in Psychology (Major), International Development Studies (Major), and Behavioural Science (Minor), McGill University

RESEARCH EXPERIENCE

2021–2026	Graduate Student Researcher, Cognitive & Neural Computation Lab, University of California, Irvine
2017–2021	Graduate Student Researcher and Lab Manager, Carrasco Lab, New York University
2016–2017	Research Associate, Culture, Mind, and Brain Program, McGill University
2015–2017	Research Associate, Cognitive Electrophysiology Lab, Douglas Mental Health Institute
2014–2017	Research Associate, McGill Cognitive Neuroscience Lab

FIELD OF STUDY

Visual Perception and Metacognition

HONORS AND AWARDS

2025	UCI Tarow and Minako Indow Fellowship for Research Excellence
2021	NSERC Canada Postgraduate Scholarship – Doctoral
2019	NYU M.A. Psychology Research Conference Poster Prize
2015	McGill University Carol and Lloyd Darlington Arts Internship Award
2013	McGill University International Relations Students' Association Award
2012	McGill University Entrance Scholarship

PUBLICATIONS

Bradford, N. A., Shen, A., Odegaard, B., & Peters, M. A. K. (2024). Aligning consciousness science and US funding agency priorities. *Communications Biology*, 7(1), 1315.

Donovan, I., Shen, A., Tortarolo, C., Barbot, A., & Carrasco, M. (2020). Exogenous attention facilitates perceptual learning in visual acuity to untrained stimulus locations and features. *Journal of Vision*, 20(4), 18, 1–19.

ABSTRACT OF THE DISSERTATION

A visual field map of perceptual confidence

by

Angela Shen

Doctor of Philosophy in Cognitive Sciences

University of California, Irvine, 2026

Professor Megan Peters, Chair

Visual performance varies systematically across the visual field. These asymmetries are well established in perception, but it is less clear whether they are similarly reflected in our subjective judgments about what we see. In this dissertation, I examine the relationship between perceptual decisions and confidence in those decisions across eccentricity (distance from fixation) and polar angle (direction around fixation).

First, I measured orientation discrimination accuracy and confidence across 24 visual field locations and compared their relationship across a matched range of performance. Although accuracy showed pronounced visual field asymmetries, the relationship between accuracy and confidence was largely invariant across polar angle. Confidence therefore preserved the spatial structure of perceptual accuracy without introducing corresponding asymmetries in their relationship.

I next asked whether this stability extends across other sources of perceptual uncertainty. In a brightness comparison task, confidence increased with visual eccentricity and stimulus noise even when performance ranges were matched, and these effects depended on overall stimulus strength. Thus, confidence does not depend on accuracy alone, but integrates multiple properties of perceptual evidence.

Finally, I examined confidence as a joint function of accuracy and response speed, developing a new metric to characterize the three-dimensional relationship among them. Both independently contributed to confidence, while their relationship with confidence varied more strongly across eccentricity than across polar angle.

Together, these findings provide a systematic and comprehensive map of perceptual confidence

across the visual field, showing that confidence reflects spatial variation in visual accuracy while also being sensitive to other dimensions of perceptual information. More broadly, they suggest that metacognition neither simply reproduces nor fully compensates for visual field asymmetries, but is shaped by a combination of stable and context-dependent mappings between objective performance and subjective experience.

General Introduction

An important goal in the study of visual perception is to understand how visual information is processed across the visual field, as inferred by objective perceptual task performance and subjective estimates of performance. Several factors affect visual information processing, including properties of the stimulus, such as its features, quality, and location, and properties of the observer, such as prior beliefs, individual differences, and internal sensory noise. Importantly, our visual experience and our introspection about that experience sometimes, but do not always, correspond. Visual information is inherently noisy, and this noise varies systematically across the visual field. Both visual perception and metacognition — our subjective evaluation of perception — are themselves subject to processing noise. These processes may rely on different aspects of sensory and decision information, allowing metacognition to diverge from perception.

Metacognition can be studied using subjective reports, by asking observers to evaluate a property of their percept, such as its visibility, or to evaluate their own performance on a perceptual task. One commonly used measure of metacognition is confidence: an observer's certainty that their perceptual decision is correct (for reviews, see Fleming, 2024; Mamassian, 2016; Peters, 2022; Rahnev, 2026; Yeung and Summerfield, 2012). Perceptual confidence therefore provides a window into how observers evaluate the evidence underlying their perceptual decisions that cannot be inferred from the decisions themselves. Under typical viewing conditions, confidence tracks perceptual performance: observers are generally more confident in correct than incorrect decisions, and confidence tends to increase with the strength of perceptual evidence (Baranski and Petrusic, 1994; Fleming et al., 2012, 2010; Yeung and Summerfield, 2012). However, this correspondence is not perfect. Confidence can vary even when perceptual performance is held constant (Cortese et al., 2016; Koizumi et al., 2015; Lau and Passingham, 2006; Maniscalco and Lau, 2016; Morales et al., 2022; Peters et al., 2017b; Rahnev, 2026; Samaha et al., 2016), suggesting that metacognitive judgments may depend on information beyond that reflected in perceptual accuracy.

A common approach is to titrate stimulus strength to match perceptual performance across experimental conditions and then compare confidence at the matched level. While this approach has been fruitful in disentangling these psychological processes, it has several limitations. Differences in confidence may depend on the particular level of performance at which conditions are matched, and apparent matching may sometimes reflect insufficient evidence for a small difference in perceptual performance

rather than evidence that performance is equivalent (Maniscalco et al., 2026; Morales et al., 2022). Further, varying stimulus strength to achieve matched performance can itself affect estimates of metacognitive ability (Rahnev and Fleming, 2019). A single level of matched performance may therefore obscure how the relationship between perceptual performance and confidence changes across the broader range of performance.

The relative psychometric function (RPF) framework offers an alternative approach by characterizing subjective reports across a *range* of perceptual performance rather than at a single matched level (Maniscalco et al., 2026). Psychometric functions are first fit separately to perceptual performance and subjective reports measured over the same levels of stimulus strength, and then combined to express subjective reports directly as a function of performance. The resulting RPFs can then be compared across conditions within the interval of perceptual performance shared among all conditions. The area under the RPF provides a single-number summary of this relationship, capturing differences in subjective report relative to perceptual performance.

The RPF can be used to relate different measures of metacognition to perceptual performance, of which there are many (Rahnev, 2025). One such measure, metacognitive sensitivity, captures not how confident an observer is in general, but how informative their confidence is about their perceptual performance (Clarke et al., 1959; Fleming and Lau, 2014; Galvin et al., 2003; Maniscalco and Lau, 2012, 2014). Metacognitive sensitivity can be assessed by relating confidence to a dimension of decision-making, such as accuracy or reaction time, with greater sensitivity indicating that confidence more reliably distinguishes decisions along that dimension. Importantly, an observer's overall level of confidence, sometimes described as metacognitive bias, can vary independently of their metacognitive sensitivity.

Visual perception and performance also vary systematically, but not always in concert with confidence. For most visual tasks, perceptual performance is not uniform across the visual field: it declines with eccentricity, or distance from the center of our gaze (for a review, see Strasburger et al., 2011). Performance also differs as a function of polar angle. At a fixed eccentricity, performance is typically better along the horizontal than the vertical meridian (horizontal-vertical anisotropy, HVA), and along the lower than the upper vertical meridian (vertical meridian asymmetry, VMA). These polar angle asymmetries (sometimes called performance fields; Altpeter et al., 2000; Mackeben, 1999) are reflected in the anatomical and physiological organization of the visual system, from the retina to visual cortex (for a review, see Himmelberg et al., 2023).

Polar angle asymmetries are prevalent across visual tasks, including detection, discrimination, and localization, and across a wide range of visual dimensions (review: Himmelberg et al., 2023). Their magnitude generally increases with eccentricity (Baldwin et al., 2012; Carrasco et al., 2001, 2002; Fuller et al., 2008; Greenwood et al., 2017; Jigo et al., 2023; Rijsdijk et al., 1980) and decreases with distance from the cardinal meridians, such that performance becomes more similar at intercardinal locations (Abrams et al., 2012; Altpeter et al., 2000; Baldwin et al., 2012; Barbot et al., 2021; Carrasco et al., 2001; Corbett and Carrasco, 2011; Talgar and Carrasco, 2002). These asymmetries extend beyond perceptual accuracy: the speed of information accrual also varies with polar angle, with faster processing along the horizontal meridian, intermediate processing at intercardinal locations, and slower processing along the vertical meridian (Carrasco et al., 2004). They are retinotopic (Corbett and Carrasco, 2011), monocular and binocular (Barbot et al., 2021; Carrasco et al., 2001), and symmetric about the vertical meridian such that there is no difference between the left and right hemifields (Barbot et al., 2021; Carrasco et al., 2001).

The spatial structure of perceptual performance is reflected throughout the visual system. Retinal cone and ganglion cell densities decrease with eccentricity and vary with polar angle, although these asymmetries alone cannot fully account for those observed behaviorally (Curcio and Allen, 1990; Curcio et al., 1990; Kupers et al., 2022, 2019; Watson, 2014). In early visual cortex, cortical magnification similarly decreases with eccentricity, while greater cortical surface area represents the horizontal than the vertical meridian and the lower than the upper vertical meridian (Benson et al., 2021; Himmelberg et al., 2021, 2022). The relationship between cortical magnification and other visual properties also differs across eccentricity and polar angle, suggesting that these dimensions may reflect partly distinct constraints on visual processing (Himmelberg et al., 2025). Recent modeling work supports this distinction: variation with eccentricity was associated with differences in gain, nonlinearity, and internal noise, whereas variation with polar angle was associated specifically with differences in gain (Xue et al., 2026a). Together, these findings reveal visual field asymmetries across multiple stages of visual processing, from the sensory input itself to its cortical representation and subsequent computations.

The pronounced decline in perceptual performance across eccentricity is not always mirrored by subjective judgments. Observers sometimes report greater confidence or visibility in the periphery than would be expected from their objective performance, a phenomenon known as subjective inflation (Li et al., 2018; Odegaard et al., 2018a; Okubo et al., 2026; Okubo and Yokosawa, 2023; Rahnev et al., 2011; Solovey et al., 2015; Tian et al., 2025, but see Pruitt et al., 2024; Toscani et al., 2021). Subjective inflation has

been observed across several perceptual tasks and subjective measures, indicating that the phenomenon is not specific to a single perceptual judgment or subjective report.

One account of subjective inflation attributes these dissociations to differences in the variability of perceptual evidence across conditions. When observers use a common decision criterion across conditions that differ in sensory uncertainty, greater variability in the internal response can produce inflated subjective judgments in the noisier or less reliable condition (Gorea and Sagi, 2000; Rahnev et al., 2011). Evidence for this account comes from model comparisons supporting the use of a common criterion across conditions (Morales et al., 2015) as well as studies in which experimentally increasing the variability of sensory representations decreased perceptual accuracy while increasing confidence (Peters et al., 2017b; Rahnev et al., 2012). Other models instead allow decision and confidence criteria to shift with sensory uncertainty (Adler and Ma, 2018; Denison et al., 2018), suggesting that the mapping from perceptual uncertainty to subjective judgment may itself be flexible. On either account, subjective inflation can emerge from how sensory uncertainty is incorporated into subjective judgments, rather than from perceptual performance alone.

Subjective inflation demonstrates that perceptual performance and metacognition can vary differently across eccentricity. Whether metacognition similarly reflects — or departs from — the pronounced asymmetries in perceptual performance around polar angle remains largely unexplored. More broadly, when perceptual performance varies, how does confidence vary with it? When does confidence preserve the structure of perceptual performance, and when does it contain structure that perceptual accuracy alone cannot explain?

In this dissertation, I examine how confidence relates to perceptual performance across variations in the visual information available to an observer. Chapter 1 directly tests how perceptual performance and confidence vary together around the visual field. I measured perceptual accuracy and confidence in an orientation discrimination task across 24 visual field locations spanning three eccentricities and eight polar angles. Using the RPF framework, I compared confidence across matched ranges of perceptual performance and additionally examined metacognitive sensitivity. Despite pronounced polar angle asymmetries in perceptual performance, similar levels of accuracy gave rise to similar confidence around polar angle.

Chapter 2 turns to other sources of perceptual uncertainty, asking how stimulus noise and strength influence confidence in addition to visual field location. I used a luminance comparison task in which

stimuli differed in their average luminance, luminance variability, and eccentricity, while observers judged relative brightness and reported their confidence. I show that both greater eccentricity and stimulus noise increased confidence beyond what was expected from perceptual performance, and that these effects depended on stimulus strength.

Chapter 3 expands the characterization of perceptual performance to include response speed alongside accuracy. Using the visual field dataset from Chapter 1, I modeled confidence jointly as a function of accuracy and response speed and extended the RPF framework to three dimensions. I introduce a new metric to summarize these three-dimensional confidence surfaces and show that response speed contributes to confidence beyond accuracy, while their joint association with confidence remains largely stable around polar angle.

CHAPTER 1

STABLE METACOGNITION ACROSS AN ASYMMETRIC VISUAL FIELD

1.1 ABSTRACT

Perceptual sensitivity varies systematically across the visual field, but whether metacognitive judgments reflect the same fine-grained spatial structure remains unclear. Here, we measured orientation discrimination and confidence across 24 visual field locations spanning eccentricity and polar angle. We sampled multiple stimulus strengths at each location and compared confidence over a shared range of perceptual performance, allowing us to isolate effects of visual field location from differences in objective performance. Perceptual sensitivity showed pronounced spatial asymmetries that increased with eccentricity. In contrast, confidence varied remarkably little across locations once performance was matched. Metacognitive sensitivity was similarly stable, with no systematic polar-angle asymmetries and only modest variation across eccentricity. These findings show that large, systematic differences in perceptual sensitivity are not sufficient, by themselves, to substantially alter the relationship between perception and metacognition. Instead, our results suggest that confidence largely reflects variation already present in perceptual performance, with comparatively little additional influence of visual field location on metacognitive judgments.

1.2 INTRODUCTION

Humans not only perceive the world, but also monitor the quality of those perceptions. This metacognitive ability can be expressed in confidence judgments, allowing observers to adapt when sensory or perceptual information is uncertain. An effective metacognitive system should therefore be sensitive to variation in the reliability of perceptual evidence. Understanding this relationship requires isolating confidence from perceptual performance, either by holding one constant while measuring the other, or by examining conditions in which the two naturally dissociate.

One such dissociation has been observed toward the visual periphery, where perceptual sensitivity is reduced. Several studies have reported "inflated" confidence for peripheral relative to central stimuli even after perceptual performance is matched (Odegaard et al., 2018a; Sharvashidze et al., 2025; Solovey et al., 2015), whereas others have reported underconfidence (Toscani et al., 2021) or reduced metacognitive sensitivity — the ability of confidence to distinguish correct from incorrect decisions — toward the periphery (Pruitt et al., 2024). Together, these findings suggest that visual field location can influence metacognitive judgments beyond its effects on objective perceptual performance.

However, the visual periphery is not a homogeneous sensory environment. Across diverse visual tasks, perceptual performance declines with eccentricity — or distance from the center of the visual field — but also varies systematically with polar angle (Himmelberg et al., 2023; Strasburger et al., 2011). At a fixed eccentricity, performance is typically better along the horizontal compared with the vertical meridian (horizontal-vertical anisotropy, HVA) and along the lower compared with the upper vertical meridian (vertical meridian asymmetry, VMA). These visual field asymmetries are reflected in the anatomical structure (Benson et al., 2021; Curcio et al., 1990), physiological responses (Liu et al., 2006), and computations (Kupers et al., 2022, 2019) of the visual system.

Because these asymmetries reflect systematic changes in the fidelity of sensory representations, they provide a natural test of how confidence responds to spatially structured differences in sensory reliability. Despite decades of work characterizing visual field asymmetries and evidence that transient changes in perceptual processing can disproportionately alter confidence (Rahnev et al., 2011; Tian et al., 2025), it remains unknown whether confidence is similarly shaped by stable properties of sensory processing.

If so, then confidence should vary systematically across polar angle even after perceptual perfor-

mance is matched. Alternatively, confidence may reflect spatial information more coarsely, for example by incorporating broad properties such as eccentricity, or may be spatially invariant, depending little or not at all on visual-field location once performance is accounted for.

Here, we examined the quantitative relationship between perceptual performance and confidence across 24 locations spanning eccentricity and polar angle. Rather than comparing confidence at a single matched level of performance, we sampled a range of stimulus strengths and characterized this relationship over the range of perceptual performance shared across locations. Despite pronounced spatial asymmetries in perceptual sensitivity, metacognitive measures varied remarkably little across the visual field once those asymmetries were accounted for through performance matching. These findings suggest that confidence largely reflects spatial variation already present in perception, with comparatively little additional influence of visual field location on metacognitive judgments.

1.3 Results

1.3.1 Experimental task

Observers completed a two-alternative forced-choice orientation discrimination task. Stimuli were presented at 24 visual field locations defined by three eccentricities (2, 5, and 8 dva) and eight polar angles (0°, 45°, 90°, 135°, 180°, 225°, 270°, or 315°). Polar angle varied between blocks of trials, whereas eccentricity varied pseudorandomly within blocks. On each trial, the possible target locations were marked by placeholders to minimize location ambiguity. All stimulus conditions were within-subjects in a 3 (eccentricity) × 8 (polar angle) × 5 (contrast) design. There were 32 trials for each stimulus value combination, resulting in 3840 trials per observer.

The target stimulus was a contrast-defined sinusoidal grating, which was pseudorandomly oriented left (-45°) or right (+45°) of vertical. To calibrate grating contrast so that discrimination performance was matched across stimulus locations, each observer completed a Bayesian QUEST adaptive staircase procedure to estimate the contrast corresponding to 75% discrimination accuracy. The fitted Weibull psychometric function was then inverted to determine the contrast values predicted to yield 55%, 65%, 75%, 85%, and 95% discrimination accuracy, spanning performance from near threshold to near ceiling.

On each trial, observers made a single response indicating both the perceived orientation and their

confidence (1–4, from "not confident at all" to "very confident"). See Methods and **Figure** 1.3 for complete stimulus and task details.

1.3.2 Visual field asymmetries persist in objective performance

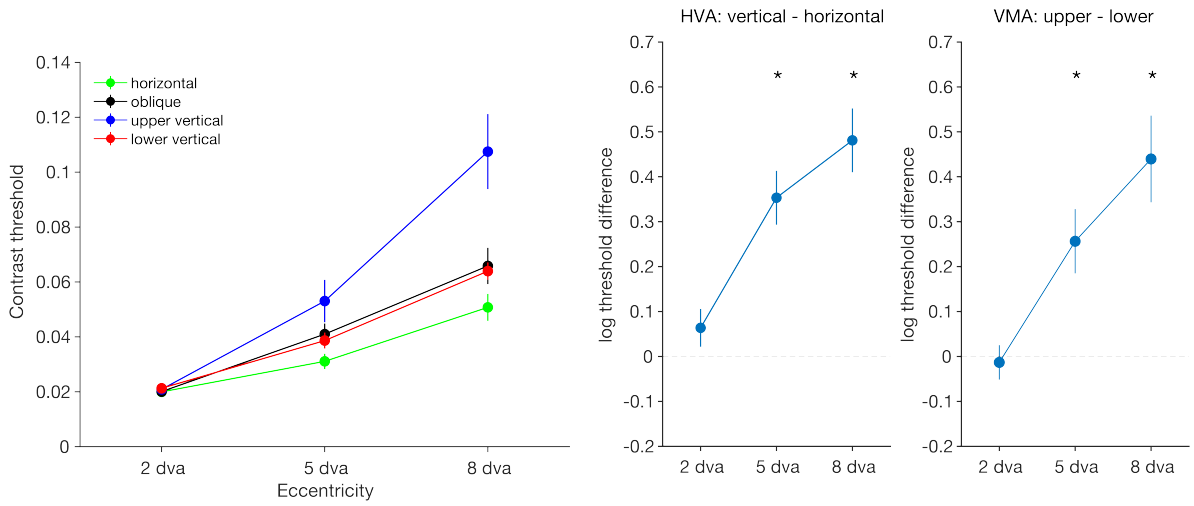

Figure 1.1: **Contrast thresholds and visual field asymmetries.** (A) Mean contrast thresholds as a function of eccentricity and meridian. Thresholds increased with eccentricity and were higher along the upper vertical meridian. Error bars indicate SEM across observers. (B) Horizontal-vertical asymmetry (HVA) and vertical meridian asymmetry (VMA) in log-transformed contrast thresholds. Positive values indicate higher thresholds along the vertical than horizontal meridian for HVA and along the upper than lower vertical meridian for VMA. Dashed lines indicate no asymmetry. *p < .05

We first confirmed the expected pattern of visual field asymmetries in contrast thresholds using the subset of locations that were thresholded individually. Threshold values varied across the visual field (**Figure 1.1A**), with significant main effects of angle ($F(3,154)=34.751$, $p<.001$, $\eta_p^2=0.40$), eccentricity ($F(2,154)=562.902$, $p<.001$, $\eta_p^2=0.88$), and their interaction ($F(6,154)=7.882$, $p<.001$, $\eta_p^2=0.23$). To interpret this interaction, we quantified the horizontal-vertical asymmetry (HVA) and vertical meridian asymmetry (VMA) from the threshold estimates.

HVA increased with eccentricity ($F(2,28)=17.004$, $p<.001$, $\eta_p^2=0.55$; **Figure 1.1B**). Planned comparisons indicated no HVA at 2 dva ($p=.288$), but significant HVA at 5 dva ($t(38)=5.983$, $p<.001$) with vertical thresholds exceeding horizontal thresholds by 42% (95% CI [26%, 60%]) and an even greater HVA at 8 dva ($t(38)=8.147$, $p<.001$), where vertical thresholds exceeded horizontal thresholds by 62% (95% CI [44%,

82%]).

VMA similarly increased with eccentricity ($F(2,28)=15.264$, $p<.001$, $\eta_p^2=0.52$). Planned comparisons indicated no VMA at 2 dva ($p=.857$), but significant VMA at 5 dva ($t(33.3)=3.516$, $p=.003$) with upper vertical thresholds exceeding lower vertical thresholds by 29% (95% CI [11%, 50%]) and an even greater VMA at 8 dva ($t(33.3)=6.029$, $p<.001$), where upper vertical thresholds exceeded lower vertical thresholds by 55% (95% CI [34%, 80%]).

Together, this pattern of results confirmed pronounced visual field asymmetries in orientation discrimination sensitivity, with both HVA and VMA increasing with eccentricity.

1.3.3 The relationship between confidence and performance shows little evidence of systematic visual field asymmetries

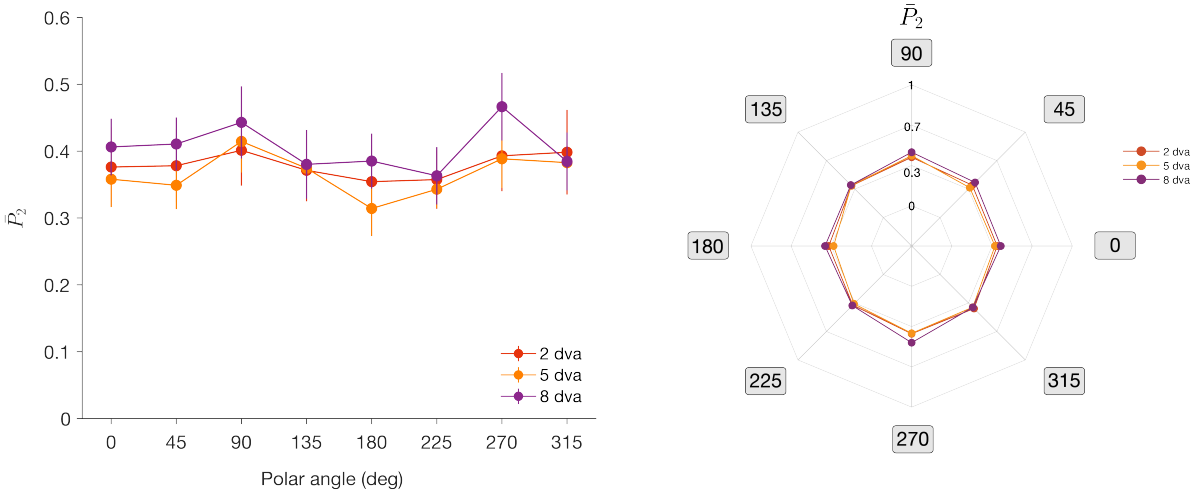

Figure 1.2: **Confidence for matched performance range across the visual field.** (A) Mean confidence conditional on matched task accuracy ($\bar{P}_2$) as a function of polar angle and eccentricity. Error bars indicate SEM across observers. (B) The same values plotted according to their corresponding locations on the visual field. $\bar{P}_2$ was largely similar across eccentricities and polar angles.

Because contrast was adjusted independently at each location, performance accuracy was broadly equated across the visual field during the main task (**Figure** 1.2). Confidence could therefore be compared over the widest performance interval that could be matched across all conditions. For each visual field location, we computed the $\bar{P}_2$ metric of the relative psychometric function, quantifying the average confi-

dence normalized by the shared range of performance across conditions being compared (Maniscalco et al., 2026, see Methods). Higher $\bar{P}_2$ values indicate greater confidence after controlling for objective performance.

If visual field location systematically altered confidence beyond its effects on perceptual performance, we would expect $\bar{P}_2$ to differ systematically across eccentricity and/or polar angle. However, the performance-matched confidence metric ($\bar{P}_2$) showed a modest effect of polar angle (F(7,97.71)=2.60, p=.017, η_p^2=0.16) and no effect of eccentricity (F(2,27.94)=1.56, p=.229, η_p^2=0.10). There was no evidence for an angle × eccentricity interaction (F(14,194.63)=0.77, p=.697, η_p^2=0.05). Bayesian model comparison provided only limited evidence for including polar angle (BF_{10}=1.37), moderate evidence for including eccentricity (BF_{10}=7.54), and strong evidence favoring the additive model over one including the interaction (BF_{01}=109.13).

Estimated marginal means were similar across eccentricities (2 dva: EMM=0.379; 5 dva: EMM=0.366; 8 dva: EMM=0.408), and no Tukey-adjusted pairwise comparison reached significance for either eccentricity or polar angle (all pairs p>.05).

Together, these findings indicate that confidence remained broadly stable across the visual field after controlling for objective performance.

1.3.4 Metacognitive sensitivity is relatively stable across the visual field after accounting for perceptual performance

We next examined whether metacognitive sensitivity varied across the visual field after matching objective performance. Such differences would indicate that visual field location influences metacognitive sensitivity beyond its effects on perceptual sensitivity. We constructed relative psychometric functions relating the area under the type 2 receiver operating characteristic curve (AUROC2) to accuracy and quantified their $\bar{P}_2$ over the shared range of accuracy across conditions (see Methods). We found no evidence that metacognitive sensitivity differed by polar angle (p=.763), eccentricity (p=.166), or their interaction (p=.562). Bayesian analyses provided strong evidence against effects of polar angle (BF_{01}=157.93) and the polar angle × eccentricity interaction (BF_{01}=38.21), whereas evidence regarding an effect of eccentricity was inconclusive (BF_{10}=1.08).

We then asked whether the same pattern held using a model-based estimate of metacognitive

sensitivity. Specifically, we used isotonic regression to derive relative psychometric functions relating *meta-d'* to *d'* and quantified their $\bar{P}_2$ over a shared range of perceptual sensitivity. Here, we found no effect of angle (p=.600) but a significant main effect of eccentricity (F(2,28.07)=3.56, p=.042, η_p^2=0.20). The interaction between angle and eccentricity was not significant (p=.973). Bayesian model comparison showed strong evidence against including angle (BF_{01}=100.43) but strong evidence in favor of including eccentricity (BF_{10}=41.75), and strong evidence favoring the additive model over the interaction model (BF_{01}=175.70).

Estimated marginal means suggested lower metacognitive sensitivity at 5 dva (EMM=1.15) than at 2 dva (EMM=1.25) and 8 dva (EMM=1.44). Tukey's adjusted pairwise comparisons revealed a significant difference only between 5 and 8 dva (t(28.1)=-2.64, p=.035); no other pairwise comparisons were significant (p>.05). Thus, although metacognitive sensitivity varied with eccentricity overall, the effect was modest and was primarily driven by lower sensitivity at the intermediate eccentricity.

Overall, both measures converged on the conclusion that metacognitive sensitivity was largely invariant across the visual field when performance is matched. Although the model-based analysis revealed modestly lower metacognitive sensitivity at the intermediate eccentricity, the effect was small and was not accompanied by systematic polar-angle differences or an angle-by-eccentricity interaction.

1.4 Discussion

Confidence is widely thought to provide an estimate of the quality of sensory evidence available for a perceptual decision (Fleming, 2024; Kepecs and Mainen, 2012; Mamassian, 2016; Rahnev, 2026). Here, we tested whether the computation relating perceptual evidence to confidence depends on where in the visual field that evidence is acquired. Despite pronounced spatial asymmetries in perceptual sensitivity, the relationship between perceptual performance and confidence varied remarkably little across visual field locations. Metacognitive sensitivity was similarly stable after differences in perceptual sensitivity were accounted for. Together, these findings suggest that large, systematic differences in sensory fidelity do not necessarily produce corresponding differences in the mapping between perception and metacognition.

Models developed to account for accuracy-confidence dissociations propose different transformations between sensory encoding and confidence generation (Shekhar and Rahnev, 2023). Although our

results do not distinguish among specific models of confidence generation, they impose an important constraint. A successful model must explain how highly location-dependent sensory representations (Xue et al., 2026b) can support comparatively location-invariant metacognitive computations.

Our findings do not imply that confidence is constant across the visual field, but rather that location has comparatively little influence on confidence beyond its effects on perceptual sensitivity. When perceptual performance is allowed to vary naturally across locations, confidence should therefore inherit the spatial asymmetries present in perception. Such asymmetries in confidence need not reflect an additional location-dependent metacognitive process, but can arise from a comparatively stable relationship between perceptual evidence and confidence.

Importantly, our task did not directly manipulate sensory or perceptual noise, but instead leveraged stable differences in sensory quality across the visual field. This distinction may help explain why large differences in perceptual sensitivity were not accompanied by the confidence inflation observed in other paradigms. Inflation has been repeatedly demonstrated under attentional manipulations, which can produce metacognitive judgments that outstrip perceptual performance (Li et al., 2018; Rahnev et al., 2011; Tian et al., 2025; Vandenbroucke et al., 2014). Inflation can also arise from experimentally imposed variation in stimulus reliability (Shen and Peters, 2026). Across these paradigms, the information available for perceptual decisions changes with experimental context. In contrast, the spatial differences leveraged here are a persistent feature of the visual system. Previous work has proposed that mismatches between expected and experienced perceptual noise can contribute to confidence inflation (Winter and Peters, 2022). Our results raise the possibility that metacognitive computations become calibrated to stable differences in perceptual sensitivity, even when they imperfectly accommodate context-dependent changes in perceptual evidence.

We note that metacognitive sensitivity as measured by *meta-d'* was lower in the middle eccentricity than in the parafovea or farther periphery, indicating that invariance is not absolute. However, this variation was considerably smaller than the corresponding effect of eccentricity on threshold sensitivity and was not observed in AUROC2. At larger eccentricities (>10 dva), *meta-d'* has been shown to decrease with eccentricity at a rate consistent with *d'* (Pruitt et al., 2024), suggesting that metacognitive sensitivity may continue to track changes in perceptual sensitivity beyond the range tested here. The present findings therefore establish relative rather than absolute invariance, demonstrated here within a single perceptual task and stimulus class. Future work should determine which changes in perceptual evidence preserve

this relationship and which alter it, including whether the stability observed here generalizes across stimulus classes, perceptual tasks, and broader ranges of the visual field.

Large differences in perceptual sensitivity are not, by themselves, sufficient to substantially alter the relationship between perception and metacognition. Rather than asking whether confidence differs across the visual field, our results suggest a different question: how does the brain transform highly variable sensory representations into comparatively stable metacognitive judgments?

1.5 METHODS

1.5.1 Observers

Fifteen observers (11 females, 4 males; mean age = 22.2 years) participated in this study. All observers had normal or corrected-to-normal vision and were naive to the purposes of the study. All observers provided informed written consent under a protocol approved by the University of California Irvine Institutional Review Board and were paid $15/hour for their participation and a $20 completion bonus.

1.5.2 Apparatus

We generated stimuli on a Dell Inspiron 5680 PC computer running Windows 10. Stimuli were displayed on a CRT monitor (NEC MultiSync FE2111SB) with a resolution of 1280 x 1024 pixels and a refresh rate of 75 Hz. The monitor was gamma-corrected using a Konica Minolta LS-100 Luminance Meter (Tokyo, Japan) with 8-bit accuracy. Observers sat in a dark and sound-attenuated room and viewed the display at a distance of 75 cm, with their heads stabilized by a chin rest. Binocular eye position was monitored using an infrared eye tracker (LiveTrack Lightning, Cambridge Research Systems, Rochester, Kent, United Kingdom) at 500 Hz to ensure fixation. Stimuli were generated using MATLAB (MathWorks, Natick, MA) and Psychtoolbox, and presentation timing was precisely controlled using a VPixx DATAPixx.

1.5.3 Main task

Design

Observers performed a two-alternative forced-choice orientation discrimination task, in which they reported whether a sinusoidal grating (4 cycles/degree) was tilted to the left or right of vertical. The experiment used a 3 (eccentricity) × 8 (polar angle) × 5 (contrast) within-subjects design.

Each block tested a single polar angle (0°, 45°, 90°, 135°, 180°, 225°, 270°, or 315°), whereas eccentricity and contrast varied pseudorandomly across trials within a block. Blocking by polar angle prevented eccentricity from being confounded with changes in the size of the attended region. The eccentricity of the grating corresponded to the center of the grating and was located at 2, 5, or 8 dva.

We used the method of constant stimuli. For each observer, five contrast values were tested at every location (see Thresholding below). The order of stimulus conditions was pseudorandomized, although the contrast values themselves differed across observers because they were determined individually during thresholding. In the main task, there were 32 trials per condition, resulting in 3840 trials per observer. Observers completed the experiment in an average of 8 one-hour experimental sessions.

Stimuli

All stimuli were presented on a medium gray (RGB color values [127.5, 127.5, 127.5]) display background. Observers maintained their gaze on a white circle with radius 0.3 dva that remained at the center of the screen throughout the entire experimental session.

Three circular placeholders were present on the screen at all three possible stimulus locations within a trial (i.e., evenly spaced at 2 dva, 5 dva, and 8 dva). The placeholders were darker gray circles (RGB values [100, 100, 100]) with a diameter of 1.6 dva and line width of 3 pixels. The distance between the placeholders and the edge of the grating was 0.05 dva and did not overlap. We used placeholders to minimize ambiguity about the possible stimulus locations. The placeholders remained on the screen throughout the trial, to avoid a potential exogenous attentional cueing effect that could have occurred if they transiently appeared and then disappeared.

The stimulus was a sinusoidal grating with a spatial frequency of 4 cycles/degree, windowed by a Gaussian envelope with a standard deviation of 0.9 grating periods (0.225 dva). The Gabor texture was contained within a circular region with a radius of 1.5 dva, and its center was positioned at an eccentricity

of 2, 5, or 8 dva. Its spatial phase was sampled independently on each trial from a uniform distribution spanning 0 to 2π. The grating was oriented 45° clockwise or counterclockwise from vertical, with the two orientations presented pseudorandomly and with equal probability.

Trial sequence

Each trial was initiated by a fixation for 300 to 500 ms. After the fixation period, the grating stimulus appeared for 100 ms at one of the three possible locations at the polar angle for that block of trials. Following the grating stimulus, there was a 200 ms delay, and then a response cue appeared. The response cue was a change in the placeholder color to blue (RGB values [50, 150, 180]) at the location of the grating only. We used a response cue to eliminate ambiguity about where the stimulus had appeared. The response cue stayed on the screen until observers gave their response, for a maximum response time window of 2000 ms. Observers simultaneously reported the orientation of the grating and their confidence level using a keyboard button press. There were four possible confidence levels, ranging from "not confident at all" to "very confident" that the orientation report is correct. If there was an eye blink or deviation >1 dva from fixation, or there was no response recorded within the response time window, the trial immediately aborted and was repeated at the end of the block. After the observer gave their response, there was a 200 ms intertrial interval, and the next trial began. No feedback was given in this task.

Observers were instructed to be as accurate as possible in their orientation judgments and as precise as possible in reporting their confidence. The trial sequence is presented in **Figure** 1.3.

Practice

Before the thresholding and main experimental sessions, observers completed three practice blocks of ten trials per block to familiarize themselves with the task procedure. The first practice block was slowed down and easy: the grating contrast was set to 0.1 and the durations of the grating presentation and the response window were three times those in the main task. The second practice block was easy (grating contrast = 0.1) and had the same stimulus timing as in the main task. The third practice block employed the same stimulus timing and was more difficult, with grating contrast set to one of five contrast levels from 0.01 to 0.1 in logarithmic steps. The polar angle for the practice blocks was 112.5°, which was not a polar angle that was tested in the main task.

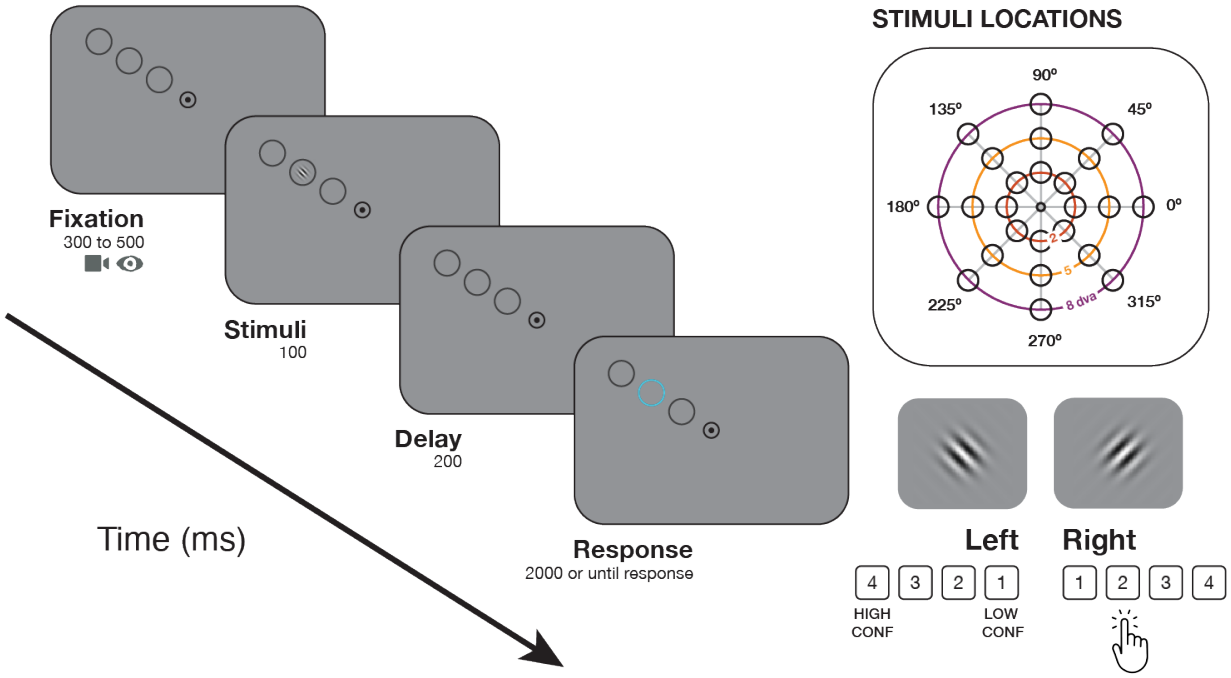

Figure 1.3: **Trial sequence and stimuli.** Three location placeholders remain on the screen for the duration of the trial. Each trial begins with a fixation period. A sinusoidal grating appears at one of three locations, and is oriented left or right of vertical. Following a delay, a response cue indicated the location at which the grating had appeared. Observers reported the tilt orientation of the grating and their confidence level simultaneously, using one of eight response keys. **Inset:** All tested stimulus locations. Polar angle was blocked, such that stimuli appeared at the same polar angle throughout each block. Within each block, stimuli could appear at one of three eccentricities.

1.5.4 Thresholding

Because contrast sensitivity varies systematically across the visual field, contrast thresholds were first estimated to equate objective discrimination performance across locations. Each observer completed a Bayesian QUEST adaptive staircase procedure, implemented using the Palamedes toolbox (Prins and Kingdom, 2018), to estimate the contrast corresponding to 75% discrimination accuracy. At each thresholded location, three independent QUEST staircases were interleaved for a total of 90 trials (30 trials per staircase). On each trial, one staircase was selected pseudorandomly, the stimulus was presented at that staircase's current threshold estimate, and the staircase was updated according to the observer's response.

To reduce thresholding time, only four polar angles were thresholded for each observer. Thresholds were measured at one horizontal meridian (randomly selected between 0° and 180°), one oblique meridian

(randomly selected among 45°, 135°, 225°, and 315°), the upper vertical meridian (90°), and the lower vertical meridian (270°). Stimulus contrast was titrated independently for each of the three eccentricities at each of the four polar angles. In total, there were 12 thresholding blocks for each observer, corresponding to the 12 thresholded visual field locations. If the individual thresholding tracks did not converge for a given location, observers repeated thresholding for that location.

The adaptive procedure estimated a posterior distribution over the threshold parameter of a Weibull psychometric function. Using the posterior median threshold estimate and fixed values for the slope, guess-rate, and lapse-rate parameters, we inverted the psychometric function to obtain stimulus contrasts corresponding to 55%, 65%, 75%, 85%, and 95% predicted discrimination accuracy. These five contrast levels were used in the main experiment to sample psychometric performance over a broad range while avoiding floor and ceiling effects.

For locations that were not thresholded directly, contrast levels were assigned from the corresponding thresholded polar angle. Specifically, thresholds obtained for one horizontal meridian were applied to the opposite horizontal meridian, and thresholds obtained for one oblique meridian were applied to the remaining oblique meridians.

1.5.5 Data analysis

Visual field asymmetry in performance

To quantify the horizontal–vertical asymmetry (HVA) and vertical meridian asymmetry (VMA), we computed subject-level log-threshold contrast scores. HVA was defined as the mean log threshold across the upper and lower vertical meridians minus the horizontal meridian, and VMA as the upper minus lower vertical meridian. These contrast scores were analyzed using linear mixed-effects models with eccentricity as a fixed effect and observer as a random intercept. Planned tests compared the estimated marginal mean contrast at each eccentricity against zero, with Holm correction across the three eccentricities.

Relative psychometric function framework

To quantify the relationship between objective and subjective measures, we employed the metaperceptual relative psychometric function (RPF) framework (Maniscalco et al., 2026). In this study, objective measures were derived from observers' discrimination performance (i.e., correct and incorrect responses),

whereas subjective measures were derived from their confidence ratings. Generally, the RPF describes the relationship between two monotonic functions that share a common independent variable. In the present study, the shared variable was stimulus contrast. The RPF can be written as:

$$\begin{aligned} R &= F_s \circ F_p^{-1} \\ R(y_p) &= F_s(F_p^{-1}(y_p)) \end{aligned} \tag{1.1}$$

where $F_p(x)$ is a function that maps contrast (x) to the objective measure y_p, and $F_s(x)$ maps contrast to the subjective measure y_s. Assuming F_p is monotonic over the range of interest and therefore invertible, F_p^{-1} gives the contrast associated with a given objective measure. The specific forms of F_p and F_s depended on the objective and subjective measures being analyzed and are described below.

The RPF analytic method therefore expresses the subjective measure directly as a function of the objective measure. To summarize the RPF, we computed $\bar{P}_2$, the area under the RPF curve across a fixed range of objective measure levels that was common to all conditions, normalized by the width of that interval. $\bar{P}_2$ can be written as:

$$\bar{P}_2 = \frac{1}{b-a}\int_a^b R(y_p)\,dy_p \tag{1.2}$$

The objective performance interval $[a, b]$ common to all conditions was defined as:

$$\begin{aligned} a &= \max_i\{\min(y_{p,i})\} \\ b &= \min_i\{\max(y_{p,i})\} \end{aligned} \tag{1.3}$$

where the lower bound a is the largest lower bound and b is the smallest upper bound across all conditions i.

Thus, $\bar{P}_2$ represents the mean value of the subjective measure over the matched objective range. A higher $\bar{P}_2$ value for a given condition indicates higher values of the subjective measure in that condition, after matching the objective measure across all conditions.

Estimation of $\bar{P}_2$ required a common objective range across all conditions within each observer. Two observers each had one location-specific condition that prevented estimation of a common performance range. For one observer, performance remained near chance across all tested contrasts at a single location, precluding reliable estimation of a function associated with the objective measure for that location. For

the second observer, two conditions had nonoverlapping performance ranges, resulting in no common range when both were included. Excluding either condition produced a common range of identical width. We therefore omitted the condition for which the fitted psychometric function provided the poorer description of the observed data. All other data were retained.

Performance and confidence

For each observer and each of the 24 visual field locations, we fit Weibull psychometric functions to the proportion correct as a function of contrast using maximum likelihood estimation in the Palamedes toolbox (Prins and Kingdom, 2018). The guess rate parameter (γ) was fixed at 0.5, and threshold (α), slope (β), and lapse rate (λ) were estimated from the data.

Mean confidence was calculated separately for each observer, location, and contrast level by averaging confidence ratings across trials. Confidence psychometric functions were then fit analogously using Weibull functions, except that all four parameters, i.e. including guess rate, were free.

Mean confidence RPFs were constructed by pairing the fitted confidence Weibull with the fitted performance Weibull. $\bar{P}_2$ quantified mean confidence over the matched performance range.

Nonparametric metacognitive sensitivity

We quantified metacognitive sensitivity using the type 2 area under the receiver operating characteristic curve (AUROC2), a nonparametric measure of the extent to which confidence discriminates correct from incorrect responses. For each condition, AUROC2 was linearly interpolated across contrast levels and paired with the corresponding performance Weibull psychometric function, yielding AUROC2 as a function of objective performance. $\bar{P}_2$ was then computed over the observer-specific range shared across all conditions.

AUROC2 could not be estimated at contrast levels containing exclusively correct or exclusively incorrect responses; these undefined values were omitted prior to interpolation. Conditions with fewer than two valid AUROC2 estimates were excluded from this analysis; no additional conditions met this criterion beyond the two observer-location cells excluded a priori.

Model-based metacognitive sensitivity

In this analysis, the RPF related perceptual sensitivity (*d'*) to metacognitive sensitivity (*meta-d'*), with (*d'*) as the objective measure and (*meta-d'*) as the subjective measure. *Meta-d'* is a model-based estimate of metacognitive sensitivity expressed in the same units as *d'*, permitting direct comparison between perceptual and metacognitive sensitivity (Maniscalco and Lau, 2012). For each condition, *d'* was first estimated across contrast levels. Because sampling variability can produce nonmonotonic estimates of *d'* as contrast increases, we applied non-decreasing isotonic regression to obtain a monotonic estimate of *d'* (Maniscalco et al., 2026).

Isotonic regression can produce repeated fitted *d'* values (plateaus). In these cases, the corresponding *meta-d'* estimates were averaged before interpolation so that each fitted *d'* value was associated with a single *meta-d'* value. The resulting interpolated *meta-d'* function was paired with the fitted *d'* function to construct the RPF, and $\bar{P}_2$ was computed over the matched performance range.

1.5.6 Statistical analysis

Linear mixed-effects models with subject random intercepts were performed in R (v4.6.1) using the lme4 (Bates et al., 2015) and lmerTest (Kuznetsova et al., 2017) packages, to evaluate the effects of polar angle and eccentricity on $\bar{P}_2$. The within-subject factors included polar angle (0°, 45°, 90°, 135°, 180°, 225°, 270°, or 315°) and eccentricity (2, 5, and 8 dva). Omnibus ANOVAs were conducted using Satterthwaite approximations for degrees of freedom. Partial η^2 is reported as a measure of effect size. Significant effects were followed by pairwise comparisons of estimated marginal means with Tukey adjustment for multiple comparisons, using the emmeans package in R (Lenth and Piaskowski, 2026). To quantify evidence for both the presence and absence of effects, we additionally computed Bayes factors using the BayesFactor package (Morey and Rouder, 2026) in R by comparing nested models with and without each effect of interest. Bayes factors are reported as BF_{10} when quantifying evidence for the alternative hypothesis and BF_{01} when quantifying evidence for the null hypothesis.

ACKNOWLEDGMENTS

We acknowledge the support of the Natural Sciences and Engineering Research Council of Canada (NSERC) Postgraduate Scholarship-Doctoral (to A.S.) and the Canadian Institute of Advanced Research (fellowship in Brain, Mind, & Consciousness, to M.A.K.P.). The funders played no role in the design, conduct, or reporting of this study.

CHAPTER 2

STIMULUS PROPERTIES AND VISUAL FIELD LOCATION INTERACT TO DRIVE PERFORMANCE-INDEPENDENT PERCEPTUAL CONFIDENCE

2.1 ABSTRACT

Perceptual confidence tracks decision accuracy, yet it is also systematically shaped by both stimulus properties and spatial location. Using a luminance comparison task, we assessed how multiple stimulus dimensions influence observers' relative brightness judgments and perceptual confidence. These dimensions included visual field location (eccentricity and polar angle) in Experiments 1 and 2, and additionally stimulus noise and overall stimulus strength in Experiment 1. We applied the recently developed *relative psychometric function* approach to characterize these dimensions' effects on confidence across a range of matched task accuracies, rather than at a single fixed performance level. Observers' confidence increased with both stimulus noise and visual eccentricity, even as performance range was matched across all conditions. These effects depended on stimulus strength – i.e., the overall luminance of the stimuli – revealing interactions among different sources of uncertainty in shaping metacognitive judgments. Together, these results extend previous accounts of the relationship between confidence and accuracy to reveal integration of multiple uncertainty sources and to include suprathreshold stimuli in brightness perception.

2.2 INTRODUCTION

Our experience of the visual world is often accompanied by a subjective sense of certainty, or *perceptual confidence*. While perceptual confidence typically covaries with decision variables such as task accuracy or reaction time (Baranski and Petrusic, 1994; Yeung and Summerfield, 2012), it is often thought to be a distinct process that reflects the probability that our visual judgment is veridical (reviews: Fleming, 2024; Mamassian, 2016; Miyoshi et al., 2024; Rahnev, 2026, 2021). Perceptual confidence and task performance rely on at least partially physiologically dissociable regions (Lau and Passingham, 2006; Pereira et al., 2020; Peters et al., 2017a; Rahnev et al., 2012; Rounis et al., 2010; Samaha et al., 2017), may rely on distinct sources of perceptual evidence (Maniscalco et al., 2021, 2016; Zylberberg et al., 2012), and have been proposed to arise from at least partially independent computational processes (Adler and Ma, 2018; Aitchison et al., 2015; Boundy-Singer et al., 2023; Cleeremans et al., 2007; Fleming and Daw, 2017; Hangya et al., 2016; Hellmann et al., 2024; Jang et al., 2012; Maniscalco and Lau, 2016; Pleskac and Busemeyer, 2010).

Many stimulus and task manipulations have been found to be useful for isolating processes driving perceptual confidence from those driving task performance so that their potentially unique computations and neural correlates may be characterized (see Peters, 2022; Rahnev, 2026, for thorough discussions). A common experimental approach is to titrate some stimulus dimension (e.g., luminance, contrast, noise, timing, or motion coherence parameters) or task condition (e.g., spatial attentional deployment) such that performance is matched between experimental conditions while allowing subjective judgments such as confidence ratings to vary (Morales et al., 2022). These approaches have yielded several consistent findings.

First, across conditions with matched discrimination performance (i.e., equated signal-to-noise ratio), increasing the total amount of sensory evidence available (*stimulus strength*) results in higher perceptual confidence (Ko et al., 2022; Koizumi et al., 2015; Odegaard et al., 2018b; Samaha et al., 2016; Samaha and Denison, 2022; Samaha et al., 2019). Relatedly, many studies attribute increased confidence to the increase in the amount of evidence specifically supporting the selected stimulus identity in discrimination tasks (Maniscalco et al., 2021, 2016; Peters et al., 2017b; Zylberberg et al., 2012). This latter finding has been called the *positive evidence bias*, interpreted as confidence reflecting reliance on the magnitude

of perceptual decision-congruent evidence. Several models have been proposed to account for these findings. Confidence may reflect a confirmation bias if it depends on continued evidence accumulation after the perceptual choice (Maniscalco et al., 2021; Moran et al., 2015; Pleskac and Busemeyer, 2010). Alternatively, the confidence readout may be corrupted by multiplicative noise that follows a lognormal distribution and scales with the magnitude of the internal signal (Shekhar and Rahnev, 2021). In cases where confidence scales with stimulus strength for incorrect or unchosen responses, it may reflect either heightened sensitivity to evidence near a discrimination boundary (Boldt et al., 2025), or dependence on a weighted combination of the task-relevant decision evidence and stimulus visibility evidence (Rausch et al., 2018, 2021).

Second, the effect of the reliability of the stimulus (external, or informational noise) on perceptual confidence has been found to depend on the specific noise manipulation and the type of task used. For example, when judging the average orientation of a group of gratings, observers displayed greater overconfidence in the condition with high variability in individual gratings' orientations compared to the condition with low contrast gratings (Herce Castañón et al., 2019). In some paradigms, stimulus reliability interacts with stimulus strength: decreasing reliability (i.e., increasing noise) produces a larger increase in confidence at low relative to high stimulus strength (Zylberberg et al., 2016), and can even reverse direction to decrease confidence when stimulus strength is high (Zylberberg et al., 2014). In other paradigms, observers' overall perceptual confidence tracks performance well and decreases in conditions with lower stimulus reliability when signal-to-noise ratio is preserved or task difficulty is fixed (Boldt et al., 2017; Desender et al., 2018; Ko et al., 2022).

Third, a consistent and meaningful way in which task performance and perceptual confidence dissociate under uncertainty is in *subjective inflation*, also known as *peripheral inflation* when specific to increased uncertainty in the periphery compared to in the center of the visual field. Subjective inflation is a phenomenon in which confidence or visibility exceed what would be expected based solely on task performance in conditions with higher noise. Subjective inflation has been observed in the visual periphery relative to stimuli that are more foveal when performance was matched between the two locations (Odegaard et al., 2018a; Rahnev et al., 2011; Rajananda et al., 2017; Solovey et al., 2015; Tian et al., 2025). The shared interpretation of these studies is that internal signal variability is higher for stimuli presented in the visual periphery – similar to several of the noise manipulations described above – lending to the appearance of a liberal detection bias when observers employ a fixed criterion across low and

high noise conditions under a signal detection framework. However, these studies observed subjective inflation within a limited visual eccentricity (<12 degrees of visual angle; dva) and with low-level visual stimuli that are confined to a small area of the visual field. At greater eccentricities, observers exhibit no inflation or even underconfidence with low-level visual stimuli (Pruitt et al., 2024; Toscani et al., 2021) and overconfidence in the periphery with scene perception (Okubo et al., 2026; Okubo and Yokosawa, 2023) and scene categorization (Sharvashidze et al., 2025) where the scene occupies a larger spatial extent. These findings suggest the presence of subjective inflation may interact with engagement of global vs. local processing, or with the use of threshold vs. suprathreshold stimuli.

To date no study has characterized the relationship between objective and subjective perceptual decisions around the entire visual field, which displays systemic asymmetry. For most visual tasks, performance declines with eccentricity (for a review, see Strasburger et al., 2011) and varies as a function of polar angle. At a fixed eccentricity beyond the parafovea, task accuracy and speed is typically better on the horizontal compared to the vertical meridian (horizontal-vertical anistropy, HVA) and on the lower compared to the upper vertical meridian (vertical meridian asymmetry, VMA), and intermediate at oblique angles. Such differences are called *polar angle asymmetries* (sometimes called *performance fields*; Altpeter et al., 2000; Mackeben, 1999) and are reflected in the anatomical and physiological organization of the brain, from the retina to – and possibly beyond – the visual cortex (for a review, see Himmelberg et al., 2023). It is worth asking then whether the relationship between perceptual performance and confidence is also systemically non-uniform across the visual field, such that the degree of subjective inflation would depend on precise visual field location. In other words, do observers subjectively perceive polar angle asymmetry?

Here, we incorporate these empirical findings into an omnibus study that comprehensively assesses the influence and interaction of visual field location, stimulus strength, stimulus reliability, and task difficulty on the relationship between task accuracy and perceptual confidence. We adapted the 2-alternative forced choice luminance comparison task design from (Ko et al., 2022), which used dynamic, flickering stimuli that allow for the manipulation of the physical noise of the stimulus, such that high variability in luminance flicker corresponded to low stimulus reliability, and vice versa. We compared two levels of stimulus strength (the summed, overall luminance of the stimuli) to observe the effect of increased overall luminance on performance-relative confidence. To assess the interaction of these factors with visual eccentricity, we added visual field locations to this paradigm, such that the luminance

comparisons were made between isoeccentric stimuli in the parafovea (2 dva) or periphery (8 dva), at horizontal and vertical polar angle locations (Experiment 1) or at intercardinal polar angle locations (Experiment 2). We employed these manipulations across seven levels of task difficulty, controlled by the real difference in mean luminance between the two stimuli compared on each trial.

Crucially, previous studies that have measured perceptual confidence while "matching" task performance typically do so at one or few performance levels. The variation in confidence reports at a given matched performance level could thus depend on the absolute level of performance chosen (Morales et al., 2022). This is apparent in studies that have documented interaction effects between metacognitive reports and task condition that depended on the absolute level of the stimulus (Rahnev et al., 2011; Zylberberg et al., 2014). To address this potential limitation, we compared confidence for a matched range of performance across all conditions using the *relative psychometric function* analytic approach (Maniscalco et al., 2026).

To summarize, perceptual confidence can systematically dissociate from objective task performance under uncertainty, but the form of this dissociation depends on both stimulus properties and task context. In particular, differences in visual field location, stimulus strength, and stimulus reliability may each alter internal signal variability in ways that affect confidence beyond what is predicted by performance alone and in ways that might vary as a function of polar angle and eccentricity. To isolate these effects, we measured confidence across a matched range of task performance while independently manipulating visual field location and stimulus properties, allowing us to assess how subjective confidence varies across the entire visual field when objective performance is held constant.

2.3 Experiment 1

2.3.1 Methods

Observers

Eight observers (5 female, mean age: 25) participated in Experiment 1. All observers had normal or corrected-to-normal vision and were naive to the purposes of the study. All observers provided informed written consent under a protocol approved by the University of California Irvine Institutional Review

Board. Observers were paid $15/hour, with a $20 completion bonus at the end of the study.

Apparatus

Experiment 1 and Experiment 2 had the same apparatus. We generated stimuli on a Dell Inspiron 5680 PC computer running Windows 10. Stimuli were displayed on a cathode ray tube (CRT) monitor (NEC MultiSync FE2111SB; 1280 x 1024) using a VPixx DATAPixx to precisely control stimulus presentation timing. We gamma-corrected the monitor using a Konica Minolta LS-100 Luminance Meter (Tokyo, Japan) with 8-bit accuracy. Observers sat in a dark and sound-attenuated room and viewed the display at a distance of 75 cm, with their head position stabilized by a chin rest. Binocular eye position was monitored using an infrared eye tracker (LiveTrack Lightning, Cambridge Research Systems, Rochester, Kent, United Kingdom) at 500 Hz to ensure fixation.

Stimuli and procedure

In this two-alternative forced-choice luminance comparison task, observers indicated which of two dynamic "flickering" circular patches was brighter on average. These patches were presented equidistant from central fixation, either on the horizontal meridian, one to the left and one to the right of central fixation, or along the vertical meridian, one above and one below fixation. The location meridian (vertical or horizontal) was randomized between blocks and consistent within each block. We incorporated a 7 (relative luminance difference) × 2 (stimulus noise) × 2 (overall luminance value) × 2 (location meridian) × 2 (eccentricity) within-subjects design. Stimuli conditions except for the location meridian were randomized on each trial. We used the method of constant stimuli across stimulus values, which did not differ overall between subjects except by their pseudorandom order of presentation. There were 64 trials per stimulus combination, totaling 7168 trials across all the stimulus conditions. This translated to 8 blocks of 112 trials per experimental session, totaling 8 sessions and roughly 8 experimental hours for each observer.

To compare performance between the periphery and the parafovea, we presented the stimuli either at 8 dva or 2 dva, respectively. These eccentricities were chosen because polar angle asymmetries typically emerge beyond ~2 dva, and to avoid ceiling performance in the center of the visual field corresponding to the fovea. Each of the two circular patches subtended 2 dva and changed in luminance with every frame

refresh (every 13.3ms at 75 Hz). On each refresh, the luminance value for each patch was determined by randomly drawing values sampled from a Gaussian distribution. On each trial, the means of the two independent Gaussian distributions were set by RGB value triplets, such that one mean was always higher than the other. The two distributions had means that were both 'high' (high overall luminance; one patch was 137 and the other was 137 + the relative luminance difference) or both 'low' (low overall luminance; one patch was 77 and the other was 77 + the relative luminance difference). Their difference could be one of seven values, [5, 12, 19, 26, 33, 40, 47], with smaller values lending to higher task difficulty and lower discriminability between the patches. On any one trial, the two normal distributions had the same standard deviation which was either 'high' (high stimulus noise condition, 51) or 'low' (low stimulus noise condition, 25.5). Generating distributions were truncated such that if the sampled value on any refresh was less than 0 or greater than 255, the value was resampled. The positions of the stimuli were counterbalanced such that the brighter patch appeared equally at left and right locations, and equally at upper or lower locations.

All stimuli were presented on a black display background. Observers were instructed to maintain their gaze on a white circle with radius 0.3 dva at the center of the screen throughout stimulus presentation. If there was an eye blink or the eyes deviated >1.5 dva from fixation during the time the circular patch stimuli were on the screen, the trial immediately aborted and was repeated at the end of the block. Each trial was initiated by fixation for 400 ms. After a short 200 ms delay, the patch stimuli onset, and observers indicated which patch they perceived to be brighter on average with a keyboard button press. The stimuli offset at the time of decision. If, after 1500 ms, observers had not made a response, the trial was aborted and repeated at the end of the block. Following the perceptual brightness decision, observers reported their subjective confidence that they had chosen correctly on a numerical scale, where 1 corresponded to "not confident," 2 to "somewhat not confident," 3 to "somewhat confident," and 4 to "very confident." Confidence ratings were not required on trials in which the relative brightness decision was not made. For all other trials, if no confidence rating was reported after 1500 ms, the trial was aborted and repeated at the end of the block. After the observer reported their confidence level, there was a 250 ms intertrial interval, and the next trial began. No feedback was given in this task. The trial sequence is presented in **Figure** 2.1

Before the main experimental sessions, observers completed three practice blocks of ten trials per block to familiarize themselves with the task procedure. The first practice block was slowed down and

easy: observers had 3000 ms to report both the luminance comparison decision and the confidence rating, and the circular patches had values that were drawn from Gaussian distributions that had a large difference in their mean (50 and 200) and low standard deviation (15) relative to the values used in the main task. The second practice block was easy like the first practice block but employed the same faster timing as the main task, with 1500 ms to report the perceptual brightness decision and the confidence rating. The third practice block employed the same timing and stimulus parameters as the main task.

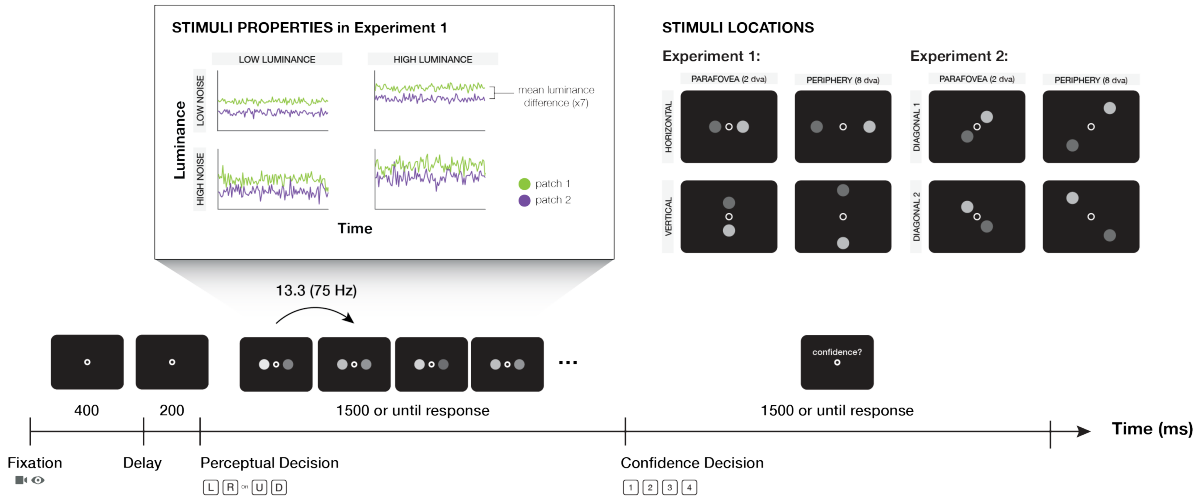

Figure 2.1: **Stimuli & trial sequence.** On each trial, two flickering circular patches appeared equidistant from center fixation at 2 dva or at 8 dva. Patch stimuli appeared in the horizontal and vertical meridians in Experiment 1, and diagonal meridians in Experiment 2. Meridian varied pseudorandomly between blocks of trials but were the same within blocks. Eccentricity varied pseudorandomly between trials. Each patch changed luminance at 75 Hz. The patches' luminance values were drawn from two independent truncated Gaussian distributions. Using a keyboard, observers were asked to indicate which patch was brighter on average, and then subsequently asked to indicate their confidence that they had responded correctly on a 4-point scale. ***Inset:*** Stimulus properties in Experiment 1. The overall mean luminance values (both high or both low) and the standard deviations (stimulus noise; both high or both low) of these two Gaussian distributions varied across trials but were the same within a trial. In Experiment 1, all four combinations of noise and luminance were included; in Experiment 2, only the low-noise, low-luminance condition was included. The distance between their mean values (relative luminance difference) could take one of seven values in a trial.

Analysis

MEASURES We collected the following measures for each condition, trial by trial: choice correctness, reaction time (RT), confidence judgment (1-4). We then computed, by condition, the performance (choice accuracy, probability of making a correct response) and the mean confidence judgment. Reaction time (RT) was log-transformed and then z-scored within each participant prior to statistical analysis. Two RT measures were used: mean zlog(RT) for luminance comparison decisions and mean zlog(RT) for confidence responses.

RELATIVE PSYCHOMETRIC FUNCTION ANALYSIS To quantify the relationship between objective performance and subjective confidence while controlling for differences in task accuracy across conditions, we employed the metaperceptual relative psychometric function (RPF) framework described by Maniscalco and colleagues (Maniscalco et al., 2026). The metaperceptual RPF relates objective performance to subjective confidence across an interval of performance levels matched across experimental conditions. This method is advantageous because performance and confidence tend to covary, and therefore evaluating their relationship necessitates an analytical framework that can differentiate effects of experimental manipulations on confidence from those on performance.

Conceptually, the RPF is derived by combining two functions estimated from the data: (1) a psychometric function relating stimulus level to performance (choice accuracy), and (2) a function relating stimulus level to confidence. By eliminating stimulus level (relative luminance difference) as an explicit variable and expressing confidence directly as a function of performance, the RPF provides a principled way to compare confidence across experimental conditions at matched levels of objective accuracy. This approach is particularly important in tasks where performance and confidence covary, as it avoids confounding changes in confidence with shifts in objective sensitivity.

In the present study, adequate parametric psychometric function fits could not be obtained for all observers in all conditions. To mediate, we employed the non-parametric approach described by Maniscalco and colleagues (Maniscalco et al., 2026). Specifically, for each observer and condition, we linearly interpolated performance as a function of stimulus level and confidence as a function of stimulus level across the discrete stimulus values tested. The RPF was then obtained by mapping interpolated confidence values onto interpolated performance values, yielding a piecewise linear estimate of confidence

as a function of performance.

To summarize the RPF, we computed two complementary scalar measures (Maniscalco et al., 2026). First, we calculated the relative area under the RPF curve (rAUC), defined as the area under the confidence–performance curve across a fixed interval of performance levels that was common to all conditions, relative to the maximal area under the curve that could occur for that interval. This interval was bounded by the highest minimum performance level and the lowest maximum performance level observed across conditions, ensuring that comparisons were restricted to a shared performance range. Second, we computed the normalized average confidence over this same performance interval, denoted ($\bar{P}_2$), which represents the mean confidence normalized by the width of the performance interval. Because performance ranges can differ across observers, ($\bar{P}_2$) provides a normalized summary of performance-matched confidence that is less sensitive to individual differences in psychometric slope or dynamic range.

Importantly, the interpolation-based RPF does not assume a specific parametric form for either the performance or confidence psychometric functions, making it well suited for conditions in which stimulus manipulations induce non-linear or observer-specific response patterns. This non-parametric interpolation approach has also been previously demonstrated to not produce systematic biases in estimation of the effects of interest - i.e., the systematic, quantitative relationship between performance and confidence (Maniscalco et al., 2026). (We note that, had we been able to fit all the data using psychometric functions, we might expect larger effect sizes than those reported below.)

STATISTICAL ANALYSIS For the relationship between accuracy and confidence resulting from the RPF analysis, all statistical analyses were also conducted in a repeated measures analysis of variance (rmANOVA) framework, using the two summary measures (rAUC, $\bar{P}_2$) calculated for each observer and each experimental condition as described above. To assess the effects of visual field location and stimulus manipulations on the quantitative relationship between performance and confidence, we performed separate 4-way rmANOVAs on rAUC and on $\bar{P}_2$. Each rmANOVA included the within-subject factors location meridian (horizontal vs. vertical), eccentricity (2 vs. 8 dva), stimulus noise (low vs. high), and overall luminance (low vs. high). Significant interactions were followed up by paired-sample t-tests to characterize the direction and significance of effects. All post-hoc comparisons were corrected for multiple comparisons using the Holm-Bonferroni procedure. Where appropriate, effect sizes are reported as partial eta squared (η_p^2) for rmANOVA effects and as mean differences with standard error and Cohen's d for pairwise comparisons.

2.3.2 Results

Accuracy, confidence, & their relationship

As expected, both accuracy (**Figure 2.2a**) and confidence (**Figure 2.2b**) increased as a function of relative luminance difference across all conditions and visual field locations.

The interval of choice accuracy levels shared among all conditions was between 0.6348 and 0.7754, shown in **Figure 2.2c**. In this interval, we calculated both rAUC (**Figure 2.2d**) and $\bar{P}_2$ (**Figure 2.2e**) for each condition.

For both rAUC and $\bar{P}_2$, we observed a significant main effect of stimulus noise (rAUC: $F(1,7) = 8.906$, $p = 0.020$, $\eta^2_p = 0.560$; $\bar{P}_2$: $F(1,7) = 10.543$, $p = 0.014$, $\eta^2_p = 0.601$), with higher noise resulting in higher rAUC ($t(7) = 2.984$, $p = 0.020$, Mean Difference = 0.010, $SE = 0.003$, Cohen's $d = 0.077$) and $\bar{P}_2$ ($t(7) = 3.247$, $p = 0.014$, Mean Difference = 0.143, $SE = 0.044$, Cohen's $d = 0.450$). For $\bar{P}_2$ only, a main effect of overall luminance ($F(1,7) = 5.922$, $p = 0.045$, $\eta^2_p = 0.458$) was significant, with higher luminance resulting in higher $\bar{P}_2$ ($t = 2.434$, $p = 0.045$, Mean Difference = 0.240, $SE = 0.099$, Cohen's $d = 0.759$). This effect was marginally significant for rAUC ($p = 0.069$).

We also observed a significant 2-way interaction between stimulus noise and overall luminance (rAUC: $F(1,7) = 6.499$, $p = 0.038$, $\eta^2_p = 0.481$; $\bar{P}_2$: $F(1,7) = 8.003$, $p = 0.025$, $\eta^2_p = 0.533$). This interaction was driven by stimulus noise, with lower rAUC and $\bar{P}_2$ in the low noise, low luminance condition compared to the high noise, low luminance condition (rAUC: $t(7) = -3.925$, $p = 0.009$, Mean Difference = -0.018, $SE = 0.005$, Cohen's $d = -0.134$; $\bar{P}_2$: $t(7) = -4.304$, $p = 0.004$, Mean Difference = -0.259, $SE = 0.060$, Cohen's $d = -0.816$) and to the high noise, high luminance condition (rAUC: $t(7) = -3.199$, $p = 0.048$, Mean Difference = -0.026, $SE = 0.008$, Cohen's $d = -0.196$; $\bar{P}_2$: $t(7) = -3.543$, $p = 0.028$, Mean Difference = -0.383, $SE = 0.108$, Cohen's $d = -1.209$). Additionally, for $\bar{P}_2$, the low noise, low luminance condition was significantly lower than in the low noise, high luminance condition ($t(7) = -3.332$, $p = 0.033$, Mean Difference = -0.356, $SE = 0.107$, Cohen's $d = -1.125$). This comparison was only marginally significant for rAUC ($p = 0.064$).

For $\bar{P}_2$ only, we observed a significant 2-way interaction between eccentricity and overall luminance ($F(1,7) = 7.166$, $p = 0.032$, $\eta^2_p = 0.506$); however, post-hoc comparisons revealed no significant effects. The interaction between eccentricity and stimulus noise was marginally significant for both rAUC and $\bar{P}_2$ (rAUC: $p = 0.091$; $\bar{P}_2$: $p = 0.056$). Follow-up t-tests indicated that both measures were significantly higher at 2 dva in the high noise condition compared to the low noise condition (rAUC: $t(7) = 3.561$, $p = 0.027$,

Mean Difference = 0.014, $SE = 0.004$, Cohen's $d = 0.105$; $\bar{P}_2$: $t(7) = 3.961$, $p = 0.012$, Mean Difference = 0.204, $SE = 0.052$, Cohen's $d = 0.644$). These results suggest that stimulus properties could have differing effects on the relationship between performance and subjective confidence depending on where the stimulus appeared.

There was also a 3-way interaction among location meridian, eccentricity, and overall luminance (rAUC: $F(1,7) = 9.614$, $p = 0.017$, $\eta^2_p = 0.579$; $\bar{P}_2$: $F(1,7) = 5.941$, $p = 0.045$, $\eta^2_p = 0.459$). However, post-hoc comparisons revealed no significant pairings for either rAUC or $\bar{P}_2$. Finally, we observed a significant interaction among all factors, meridian × eccentricity × noise × overall luminance (rAUC: $F(1,7) = 6.194$, $p = 0.042$, $\eta^2_p = 0.469$; $\bar{P}_2$: $F(1,7) = 9.740$, $p = 0.017$, $\eta^2_p = 0.582$).

All post-hoc t-test p-values were corrected using Holm-Bonferroni. All other effects and interactions did not reach significance ($p > 0.05$). Full statistical reports can be found in the Appendix.

Within each stimulus property condition

Given that we found differences between the low noise and low luminance condition and the other stimulus noise × overall luminance conditions, we decided to further explore by asking whether there were meaningful differences within each stimulus noise × overall luminance condition. We did so by conducting separate 2-way rmANOVAs within the low noise and low luminance condition, the low noise and high luminance condition, the high noise and low luminance condition, and the high noise and high luminance condition.

In the low stimulus noise × low overall luminance condiiton, we observed an interaction between eccentricity and location meridian for $\bar{P}_2$ ($F(1,7) = 5.7038$, $p = 4.4916$, $\eta^2_p = 0.449$). Post-hoc t-tests revealed no significant comparisons, although the comparison between the vertical meridian at 2 dva and at 8 dva was marginally significant ($p = 0.070$). This interaction was marginally significant for rAUC ($p = 0.072$). This suggests that, for a fixed interval of accuracy, confidence was trending towards being higher in the vertical periphery compared to the vertical center. The same trends were not found for the horizontal meridian. In other words, it's possible that subjective inflation could be observed in the periphery, which could depend on the polar angle of the stimuli.

We did not observe meaningful differences in either rAUC or $\bar{P}_2$ in the other stimulus property conditions (see also the Appendix for statistical reports). These findings motivated Experiment 2, where

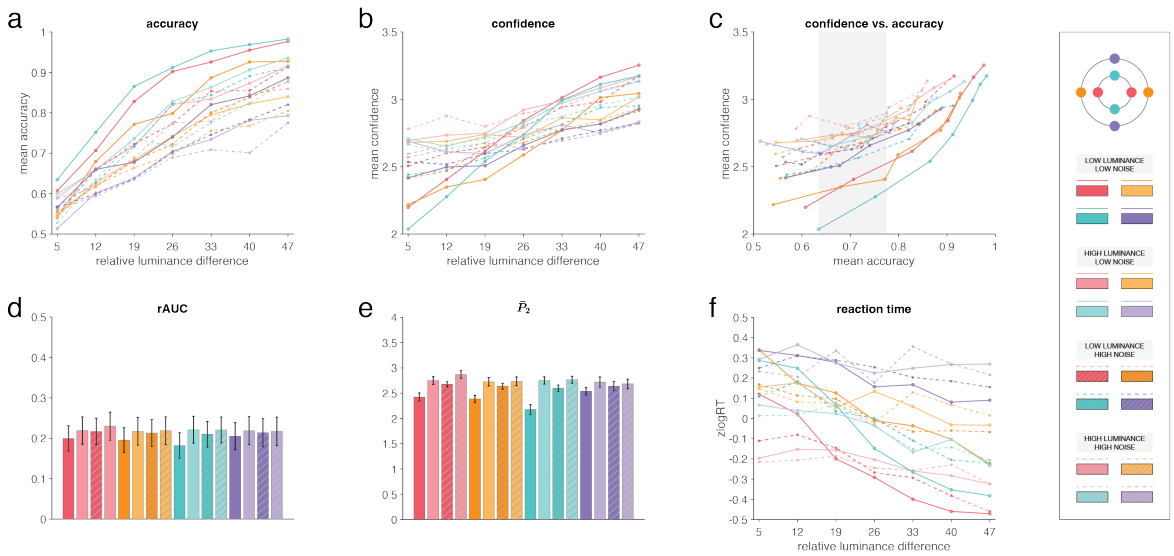

Figure 2.2: **Experiment 1 results.** The horizontal meridian at 2 dva (parafovea) and 8 dva (periphery) is represented in pink and orange, respectively. The vertical meridian at 2 dva and 8 dva is represented in blue and purple, respectively. ***a.*** Mean accuracy (i.e., probability of making a correct response) at each level of relative luminance difference. ***b.*** Mean confidence rating at each level of relative luminance difference. ***c.*** Mean confidence across mean accuracy. The shaded region represents the range of performance that was shared across all conditions. From this shaded region, rAUC (***d.***) and $\bar{P}_2$ (***e.***) were computed, with error bars denoting ±1 SEM. ***f.*** Mean reaction time in zlog units at each level of relative luminance difference. In ***a, b, c, and f***, low stimulus noise is indicated by solid lines, and high stimulus noise is indicated by dashed lines. In ***c and d***, solid bars represent low stimulus noise and hatched bars represent high stimulus noise. In all panels, darker colors represent low overall luminance, and lighter colors represent high overall luminance. In ***a, b, c, and f***, SEM was omitted for clarity.

we probed the effects of visual field location (meridian and eccentricity) at oblique polar angles while holding stimulus noise and overall luminance fixed at the low levels used in Experiment 1.

Reaction time

We performed two 4-way rmANOVAs on zlog(RT) for both luminance comparison decisions and confidence responses, with factors location meridian (horizontal or vertical), eccentricity (2 or 8 dva), stimulus noise (low or high), and overall luminance (low or high). For luminance comparison zlog(RT) **(Figure 2.2f)**, we observed a significant main effect of eccentricity ($F(1,7) = 12.342$, $p = 0.01$, $\eta_p^2 = 0.638$). Post hoc comparisons revealed significantly faster reaction times at 2 dva eccentricity in the parafovea compared to at 8 dva in the periphery (in zlog units: $t(7) = -3.513$, $p = 0.01$, Mean difference = -0.295, $SE = 0.084$,

Cohen's d = -1.412). There were trending interactions between location meridian and noise (F(1,7) = 4.131, p = 0.082), and among location meridian, stimulus noise, and overall luminance (F(1,7) = 4.094, p = 0.083). All other effects and interactions did not reach significance (p > 0.05).

For the confidence decision zlog(RT), there was an interaction between location meridian and eccentricity ($F(1,7) = 6.124$, $p = 0.043$, $\eta_p^2 = 0.467$). Post hoc comparisons revealed that this interaction was due to a significant faster reaction times between the vertical meridian at 2 dva and vertical meridian at 8 dva (in zlog units: t = -3.223, p = 0.038, Mean difference = -0.026, SE = 0.008, Cohen's d = -0.452). However, given that in this task confidence was reported after the perceptual decision, the reaction time for confidence is not likely to be a meaningful measure.

2.4 Experiment 2

2.4.1 Methods

Observers

Seventeen observers (9 females, mean age: 19.65) participated in Experiment 2. All observers had normal or corrected-to-normal vision and were naive to the purposes of the study. All observers provided informed written consent under a protocol approved by the University of California Irvine Institutional Review Board. All observers were naive to the purpose of the study and were paid $15/hour.

Stimuli and procedure

Experiment 2 has the same experimental design as Experiment 1, with the following exceptions:

1. The patch stimuli were presented at oblique polar angle locations, equidistant from the horizontal and vertical meridians. The goal of Experiment 2 was to evaluate the relationship between confidence and task accuracy at the oblique locations which have been found in previous studies to have comparable task accuracy. In each pseudorandomized block of trials, they appeared along one of the diagonal meridians: either in the upper left (135°) and lower right (315°), or in the upper right (45°) and lower left (225°), relative to central fixation. Stimulus eccentricity was the same as in Experiment 1, at 2 dva or at 8 dva.

2. Experiment 2 included only the low overall luminance condition (mean luminance of the dimmer

patch = 77) and low luminance standard deviation (25.5; low stimulus noise) from Experiment 1. These stimulus properties were selected because they produced the largest effects in Experiment 1 and allowed for a reduction in trial count. This resulted in a 7 (difference in mean luminance) × 2 (location meridian) × 2 (eccentricity) within-subject design. There were 64 trials per stimulus combination, totaling 1792 trials across all conditions. Each observer completed 8 blocks of 112 trials per session across 2 sessions (approximately 2 hours total).

Statistical analyses

All analyses proceeded as with Experiment 1, with the exception that, because Experiment 2 included only a single stimulus noise and overall luminance condition, statistical analyses were limited to the within-subject factors location meridian and eccentricity. As in Experiment 1, the relationship between performance and confidence was quantified using rAUC and the normalized average confidence over the performance interval ($\bar{P}_2$). We performed separate rmANOVAs on these measures, and on mean z-scored log reaction time.

2.4.2 Results

RPF, rAUC, and $\bar{P}_2$

We calculated RPF rAUC **(Figure 2.3d)** and RPF $\bar{P}_2$ **(Figure 2.3e)** for each condition in the shared performance interval among all conditions (0.6360 to 0.8897), shown in **Figure 2.3c**. Two-way rmANOVAs on these measures with factors location meridian and eccentricity revealed a main effect of eccentricity (rAUC: $F(1,16) = 4.84$, $p = 0.043$, $\eta_p^2 = 0.232$; $\bar{P}_2$: $F(1,16) = 5.526$, $p = 0.032$, $\eta_p^2 = 0.257$). Post-hoc comparisons showed that rAUC and $\bar{P}_2$ were significantly lower at 2 dva than at 8 dva (rAUC: $t(16)$ = -2.200, $p = 0.043$, Mean Difference = -0.028, $SE = 0.013$, Cohen's d = -0.234; $\bar{P}_2$: $t(16)$ = -2.351, $p = 0.032$, Mean Difference = -0.123, $SE = 0.053$, Cohen's d = -0.282), indicating that confidence was higher in the visual periphery than in the parafovea for the matched range of accuracy.

Location meridian and the interaction between eccentricity and location meridian were not significant, ($p > 0.05$) (see also Appendix).

Reaction time

We performed 2-way rmANOVAs on mean zlog(RT) for both luminance comparison decisions and confidence responses, with factors location meridian and eccentricity **(Figure 2.3f)**. For the luminance comparison decision, we observed a significant main effect of eccentricity ($F(1,16) = 24.829$, $p < 0.001$, $\eta^2_p = 0.608$). Reaction times were significantly faster for stimuli in the parafovea at 2 dva compared to in the periphery at 8 dva, (in zlog units: $t(16) = -4.983$, $p < 0.001$, Mean difference = -0.191, $SE = 0.038$, Cohen's $d = -1.567$). Reaction time difference between location meridians and the interaction between location meridian and eccentricity were not significant ($p > 0.05$).

The rmANOVA for zlog(RT) for the confidence responses revealed no significant effects or interactions. As in Experiment 1, reaction time for confidence is not likely to be a meaningful measure in this task paradigm.

2.5 Discussion

Visual perception is shaped by multiple sources of uncertainty, including variability in the sensory signal itself, changes in stimulus strength, and differences in how information is encoded across the visual field. While perceptual performance is known to depend on these factors, it remains less clear how they jointly influence subjective confidence *independent of performance changes* – that is, when performance is controlled for or held constant. Here, we interrogated the concurrent and interacting effects of three types of noise – stimulus reliability, overall stimulus luminance, and visual field location – on the relationship between confidence and accuracy. Across two experiments, we assessed confidence under matched ranges of perceptual performance, allowing us to isolate systematic dissociations between subjective confidence and objective task accuracy.

In both experiments, we observed systematic dissociations between subjective confidence and objective task accuracy that depended on stimulus noise, stimulus luminance, and stimulus location. In Experiment 1, increasing stimulus reliability by reducing the physical variability of stimuli luminance decreased confidence for a matched range of task accuracy. This effect interacted with overall luminance: confidence was lowest in the high reliability (low noise) and low-luminance condition, whereas the other reliability-luminance combinations produced statistically equivalent performance-matched

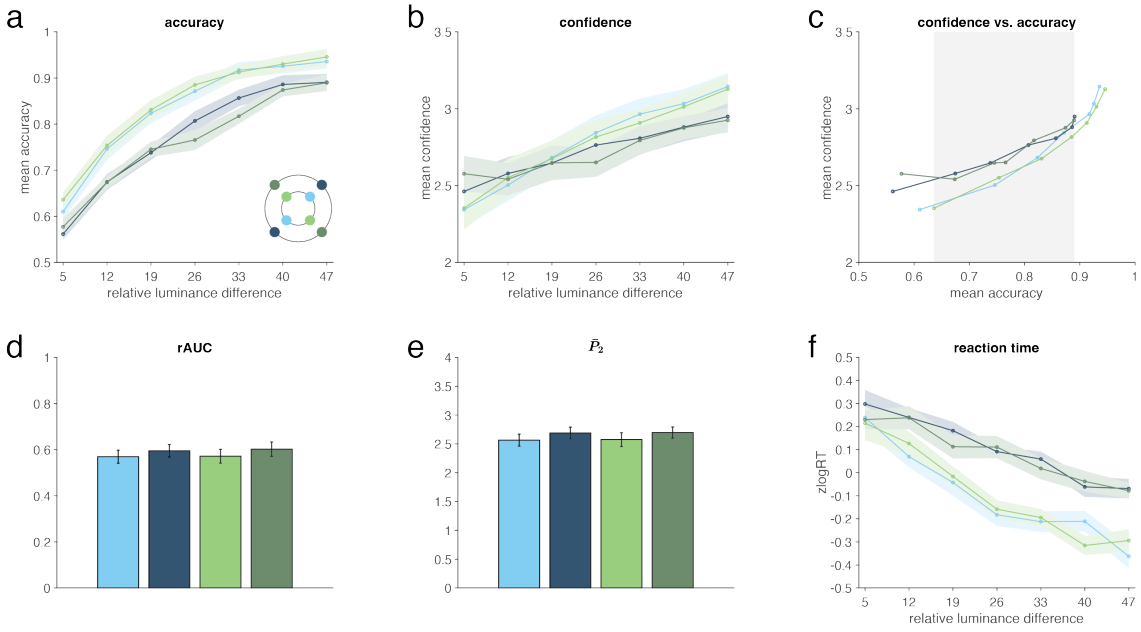

Figure 2.3: **Experiment 2 results.** The diagonal meridian that includes the lower left and upper right is represented in blue. The diagonal meridian that includes the upper left and lower right is represented in green. Lighter colors represent the parafovea at 2 dva. Darker colors represent the periphery at 8 dva. ***a.*** Mean accuracy (probability of making a correct response) at each level of relative luminance difference. ***b.*** Mean confidence rating at each level of relative luminance difference. ***c.*** Mean confidence across mean accuracy. The shaded region represents the range of accuracy that was shared for all four eccentricity × meridian conditions. From this shaded region, rAUC (***d.***) and $\bar{P}_2$ (***e.***) was computed, with error bars representing ±1 SEM. ***f.*** Reaction time in zlog units at each level of relative luminance difference. In ***a, b, and f***, shaded regions represent SEM.

confidence levels (though marginally different for the high reliability and low overall luminance condition for rAUC). This pattern is consistent with previous findings showing that the effect of stimulus reliability on confidence depends on the strength of the stimulus (Zylberberg et al., 2016, 2014).

Across both Experiments 1 and 2, observers responded faster in the parafovea (2 dva) than in the periphery (8 dva), despite matched accuracy range across locations. This pattern contrasts with prior findings suggesting that processing in the periphery can be faster, albeit at the cost of reduced accuracy (Carrasco et al., 2003; Jovanovic and Mamassian, 2019; Upadhyayula et al., 2023). Our results instead suggest that explicitly matching accuracy across eccentricities does not simply equate processing speed, but confers a speed advantage to the less peripheral location. Given evidence that confidence tends to increase as reaction time decreases (Baranski and Petrusic, 1994; Fetsch et al., 2014; Kiani et al., 2014), these

findings raise an intriguing possibility: confidence may be differentially influenced by the speed–accuracy tradeoff across the visual field. Specifically, central vision may benefit from higher accuracy at the cost of longer reaction times, whereas peripheral vision may benefit from faster responses but reduced accuracy. Future work that explicitly matches speed–accuracy tradeoffs across eccentricities would help clarify how confidence is constructed across the visual field.

Experiment 1 also revealed a reliable effect of overall luminance on confidence: observers reported higher confidence when both stimuli were brighter, even though task accuracy was matched across conditions. This finding is consistent with prior work showing that perceptual confidence increases with stimulus strength rather than solely reflecting the balance of evidence between competing alternatives (Ko et al., 2022; Koizumi et al., 2015; Miyoshi and Lau, 2020; Odegaard et al., 2018b; Peters et al., 2017b; Rausch et al., 2018; Samaha et al., 2016; Samaha and Denison, 2022; Zylberberg et al., 2012). Critically, this effect was observed across multiple levels of stimulus noise and across visual field locations, indicating that confidence covaried with stimulus strength even when signal-to-noise ratio was equated. These findings suggest that the effect of luminance on confidence – and perhaps the related effect of the positive evidence bias – may generalize across the visual field, and future studies could test this hypothesis.

In Experiment 2, we extended these findings by directly examining the effects of visual eccentricity while avoiding horizontal versus vertical meridian performance asymmetries, observing that confidence was higher for peripheral stimuli than for parafoveal stimuli at matched performance ranges, as reflected in both rAUC and $\tilde{P}_2$. Importantly, performance-matched confidence did not differ between the two oblique meridians tested, supporting accounts of polar angle asymmetry that show similar performance for stimuli placed along oblique angles (Barbot et al., 2021; Carrasco et al., 2001; Himmelberg et al., 2023).

A key methodological feature of the present work – and a key component of our resulting empirical contribution – is the use of performance matching across a continuous range of accuracy, rather than equating performance at a single operating point, or pair of points, as is typically done. We quantified confidence–performance relationships using summary measures derived from the relative psychometric function (Maniscalco et al., 2026), allowing confidence to be compared across conditions that spanned comparable performance intervals. This approach mitigates concerns associated with ceiling or floor effects that can arise when confidence is assessed at isolated accuracy levels, particularly in suprathreshold tasks. Specifically, with the exception of few studies (Tian et al., 2025), subjective inflation has only been demonstrated near threshold detection or discrimination (Li et al., 2018; Odegaard et al., 2018a; Rahnev

et al., 2011; Solovey et al., 2015). This has led to some skepticism about whether subjective inflation is relevant for everyday vision, leading to more recent studies tackling the robustness and generalizability of the effect. These efforts include a study of color sensitivity using naturalistic images, which showed that observers' bias to over-report color in the periphery scaled with the aperture of color in chimera images with a colored center and greyscaled periphery (Okubo and Yokosawa, 2023). Likewise, in the studies reported by Tian, Maniscalco and colleagues (Tian et al., 2025), subjective inflation was found for suprathreshold grating orientation discrimination for stimulus visibility ("did you see a grating?") but not for the task-relevant feature ("did you see the orientation?"). It is interesting to note that these apparent differences in the quantitative relationship between accuracy and confidence for task-relevant versus task-irrelevant stimulus manipulations have also recently been reported by other groups (Fung et al., 2025); future work will be required to better understand interactions between task-relevant or irrelevant stimulus manipulations and response prompts in driving accuracy-confidence relationships.

Importantly, our task employs suprathreshold stimuli and observers reported confidence, not visibility, as the subjective measure. We demonstrate that confidence is higher than what performance accuracy would suggest, applied to stimuli that are clearly visible to all observers. This means our results may appear to contradict those reported by Solovey and colleagues 2015, who found that subjective inflation for near-threshold stimuli can be attenuated when stimulus size is adjusted according to cortical magnification (M-scaling), thereby equalizing sensory variability across eccentricity. In the present study, stimuli were not M-scaled, and thus peripheral representations may have remained noisier than parafoveal representations at the sensory level.

Our findings have important implications for how perceptual confidence is understood and modeled. Many accounts implicitly assume that confidence reflects the precision or reliability of the underlying sensory representation or decision variable, such that increases in signal quality should monotonically increase confidence (Boundy-Singer et al., 2023; Fleming, 2024). Our results challenge this assumption by showing that confidence depends on multiple interacting sources of uncertainty or noise, including stimulus reliability, stimulus strength, and spatial location, in ways that are not reducible to objective performance alone. These robust dissociations suggest that subjective confidence is shaped by structured complexities in how perceptual evidence is evaluated, rather than serving as a simple readout of accuracy or internal noise.

Understanding these complex interactions is critical for theories of confidence, metacognition, and

decision-making that aim to explain how observers evaluate their perceptual experiences in everyday settings. Specifically, recent theoretical work has emphasized that dissociations between confidence and accuracy should not be treated as anomalies, but rather as informative signatures of how confidence is computed (Peters, 2022; Rahnev, 2026). In this framework, confidence–accuracy dissociations can arise from multiple loci, including pre-decisional sensory encoding, decision-level evidence accumulation, and post-decisional confidence readout. Importantly, the presence of a dissociation alone is insufficient to localize its underlying mechanism, as similar behavioral patterns may emerge from distinct computational processes. Instead, empirical findings constrain the class of models that can account for confidence judgments under uncertainty (Rong and Peters, 2023). Here, we observed effects of stimulus magnitude and reliability, and of visual field location – which are compatible with *both* decisional accounts that emphasize evidence accumulation dynamics and evidence weighting, and pre-decisional accounts involving attentional modulation or differential encoding across the visual field where both of these components may impact the reliability of the underlying visual representations. Although our results cannot adjudicate among such accounts – as noted by Rahnev (2026) – they nevertheless add to the growing body of empirical data that may be used to adjudicate such accounts in future.

To this end, our novel effects of polar angle as well as eccentricity on the relationship between performance and confidence may especially contribute to these ongoing debates. Specifically, in Experiment 1, we observed higher performance-controlled confidence in the vertical periphery compared to the vertical center, at low levels of stimulus noise and low overall luminance. However, this difference was not observed along the horizontal meridian. In other words, mean confidence covaried with stimulus- and eccentricity-induced performance changes in both the horizontal center and the horizontal periphery. Similarly, we also observed that mean confidence covaried with stimulus- and meridian-induced performance changes within the periphery, i.e. when comparing vertical versus horizontal peripheral locations. The differences in the performance-confidence relationship thus primarily appear when comparing parafoveal to peripheral confidence, especially in Experiment 2: performance-controlled confidence was clearly higher in the periphery, mirroring the effects seen in the low-noise, low-luminance condition in Experiment 1. (Note: direct comparisons unfortunately cannot be made between Experiments 1 and 2 because the number of trials and conditions are not matched.)

Several limitations and boundary conditions of the present work warrant consideration. First, although we manipulated stimulus location across eccentricity and polar angle, we did not directly

measure, control, or manipulate the spatial extent of attentional allocation. In particular, our use of parafoveal (2 dva) versus peripheral (8 dva) stimuli presented *across* the whole visual field – rather than, for example, at a single 8 dva location – may have created differences in the *extent* of the spatial envelope of visual attention which may have further interacted with stimulus reliability or strength in addition to eccentricity itself (Eriksen and St. James, 1986; Reynolds and Heeger, 2009). However, if anything, we believe the significantly larger spatial attention envelope in the 8 dva condition could have further degraded internal representations in the peripheral conditions rather than enhancing them – and that our performance-matching analytic approaches would account for any changes in performance related to this increased noise. Future work that more explicitly controls for or measures the extent of spatial attention would help clarify the contribution of attentional factors to performance-matched confidence differences.

Second, the generality of the present findings may be constrained by task and stimulus characteristics. We examined confidence in a perceptual comparison task involving luminance-modulated stimuli and time-extended evidence accumulation, following work established by Ko et al. (2022). While this design allowed us to probe confidence under suprathreshold conditions and across multiple sources of uncertainty, subjective inflation may depend on the specific stimulus dimension, decision structure, or response demands of the task. For example, confidence biases may differ for tasks involving categorical judgments, feature detection, or continuous estimation, or when uncertainty is introduced along different stimulus dimensions (as done by (Fung et al., 2025)). Thus, while the present results demonstrate robust confidence-accuracy dissociations under a particular set of conditions, further work is needed to determine the extent to which these effects generalize across tasks, stimulus domains, and decision contexts.

In summary, the present work demonstrates that subjective confidence can dissociate systematically from objective performance under matched accuracy range, and that these dissociations depend on interacting sources of uncertainty, including stimulus reliability, stimulus strength, and spatial location. Extending previous findings, we show that subjective inflation can be observed in a task where decision information accumulates with time, and that it generalizes beyond contrast sensitivity to include luminance as the stimulus dimension, thereby probing brightness perception. Finally, in addition to effects of eccentricity, we show that performance-controlled confidence can vary as a function of polar angle, revealing structured spatial asymmetries in confidence that are not captured by eccentricity alone.

Thus, by combining suprathreshold stimuli, time-extended evidence accumulation, and performance-range matching, this study extends prior demonstrations of subjective inflation beyond near-threshold paradigms and single-source manipulations of uncertainty. More broadly, these findings highlight the need for models of perceptual confidence that account for how multiple sources of information – including spatially structured visual field properties – are integrated and weighted when observers evaluate their own perceptual decisions.

ACKNOWLEDGMENTS

We thank Brian Maniscalco for providing fruitful discussion and guidance on the RPF method, and Tracy Chen for help with data collection for Experiment 2.

We acknowledge the support of the Natural Sciences and Engineering Research Council of Canada (NSERC) Postgraduate Scholarship-Doctoral (to A.S.) and the Canadian Institute for Advanced Research Brain, Mind & Consciousness Program (to M.A.K.P.).

2.6 APPENDIX

The following tables use these abbreviations:

- loc = location meridian
- ecc = eccentricity
- noise = stimulus noise
- lumi = overall luminance

EXPERIMENT 1 RESULTS TABLES

4-way (loc × ecc × noise × lumi) repeated measures ANOVAs

RPF rAUC

RPF rAUC			
Within-subjects effects	$F(1,7)$	p	η^2_p
loc	1.382	0.278	0.165
ecc	2.217×10^{-5}	0.996	3.167×10^{-6}
noise	8.906	0.020*	0.560
lumi	4.600	0.069	0.397
loc × ecc	1.077	0.334	0.133
loc × noise	2.079	0.193	0.229
ecc × noise	3.842	0.091	0.354
loc × lumi	0.062	0.810	0.009
ecc × lumi	3.569	0.101	0.338
noise × lumi	6.499	0.038*	0.481
loc × ecc × noise	0.915	0.371	0.116
loc × ecc × lumi	9.614	0.017*	0.579
loc × noise × lumi	1.481	0.263	0.175
ecc × noise × lumi	0.263	0.624	0.036
loc × ecc × noise × lumi	6.194	0.042*	0.469

RPF $\bar{P}_2$

RPF $\bar{P}_2$			
Within-subjects effects	$F(1,7)$	p	η_p^2
loc	0.769	0.410	0.099
ecc	0.009	0.925	0.001
noise	10.543	0.014*	0.601
lumi	5.922	0.045*	0.458
loc × ecc	1.781	0.224	0.203
loc × noise	3.045	0.125	0.303
ecc × noise	5.207	0.056	0.427
loc × lumi	9.418×10^{-4}	0.976	1.345×10^{-4}
ecc × lumi	7.166	0.032*	0.506
noise × lumi	8.003	0.025*	0.533
loc × ecc × noise	3.506	0.103	0.334
loc × ecc × lumi	5.941	0.045*	0.459
loc × noise × lumi	1.791	0.223	0.204
ecc × noise × lumi	0.724	0.423	0.094
loc × ecc × noise × lumi	9.740	0.017*	0.582

zlog(RT) for the luminance comparison decision

Reaction Time (zlogRT) for luminance comparison decision			
Within-subjects effects	$F(1,7)$	p	η^2_p
loc	2.986	0.128	0.299
ecc	12.342	0.010*	0.638
noise	0.014	0.910	0.002
lumi	0.694	0.432	0.090
loc × ecc	0.034	0.859	0.005
loc × noise	4.131	0.082	0.371
ecc × noise	0.149	0.711	0.021
loc × lumi	0.022	0.886	0.003
ecc × lumi	1.840	0.217	0.208
noise × lumi	0.915	0.371	0.116
loc × ecc × noise	0.468	0.516	0.063
loc × ecc × lumi	0.506	0.500	0.067
loc × noise × lumi	4.094	0.083	0.369
ecc × noise × lumi	0.057	0.818	0.008
loc × ecc × noise × lumi	0.048	0.833	0.007

zlog(RT) for confidence rating

Reaction Time (zlogRT) for confidence rating			
Within-subjects effects	$F(1,7)$	p	η^2_p
loc	0.057	0.819	0.008
ecc	4.262	0.078	0.378
noise	0.161	0.700	0.022
lumi	0.482	0.510	0.064
loc × ecc	6.124	0.043*	0.467
loc × noise	0.026	0.877	0.004
ecc × noise	0.112	0.747	0.016
loc × lumi	0.035	0.856	0.005
ecc × lumi	0.020	0.892	0.003
noise × lumi	4.151×10^{-5}	0.995	5.930×10^{-6}
loc × ecc × noise	0.195	0.672	0.027
loc × ecc × lumi	0.122	0.737	0.017
loc × noise × lumi	1.666	0.238	0.192
ecc × noise × lumi	1.205	0.309	0.147
loc × ecc × noise × lumi	1.457	0.267	0.172

Low noise, low luminance condition: 2-way (loc × ecc) repeated measures ANOVAs

RPF rAUC

RPF rAUC			
Within-subjects effects	$F(1,7)$	p	η_p^2
loc	1.000	0.351	0.125
ecc	3.226	0.116	0.316
loc × ecc	4.492	0.072	0.391

RPF $\bar{P}_2$

RPF $\bar{P}_2$			
Within-subjects effects	$F(1,7)$	p	η_p^2
loc	0.066	0.805	0.009
ecc	3.226	0.116	0.316
loc × ecc	5.704	0.048*	0.449

Low noise, high luminance condition: 2-way (loc × ecc) repeated measures ANOVAs

RPF rAUC

RPF rAUC			
Within-subjects effects	$F(1,7)$	p	η_p^2
loc	0.300	0.601	0.041
ecc	0.093	0.769	0.013
loc × ecc	0.016	0.903	0.002

RPF $\bar{P}_2$

RPF $\bar{P}_2$			
Within-subjects effects	$F(1,7)$	p	η_p^2
loc	0.479	0.511	0.064
ecc	0.103	0.758	0.014
loc × ecc	0.042	0.844	0.006

High noise, low luminance condition: 2-way (loc × ecc) repeated measures ANOVAs

RPF rAUC

RPF rAUC			
Within-subjects effects	$F(1,7)$	p	η_p^2
loc	1.611	0.245	0.187
ecc	0.263	0.624	0.036
loc × ecc	0.246	0.635	0.034

RPF $\bar{P}_2$

RPF $\bar{P}_2$			
Within-subjects effects	$F(1,7)$	p	η_p^2
loc	0.141	0.719	0.020
ecc	0.009	0.928	0.001
loc × ecc	0.784	0.405	0.101

High noise, high luminance condition: 2-way (loc × ecc) repeated measures ANOVAs

RPF rAUC

RPF rAUC			
Within-subjects effects	$F(1,7)$	p	η_p^2
loc	2.010	0.199	0.223
ecc	0.574	0.473	0.076
loc × ecc	0.364	0.565	0.049

RPF $\bar{P}_2$

RPF $\bar{P}_2$			
Within-subjects effects	$F(1,7)$	p	η_p^2
loc	2.886	0.133	0.292
ecc	0.784	0.405	0.101
loc × ecc	1.037	0.342	0.129

EXPERIMENT 2 RESULTS TABLES

2-way (location loc × ecc) repeated measures ANOVA on RPF rAUC

RPF rAUC			
Within-subjects effects	$F(1,16)$	p	η_p^2
loc	0.235	0.634	0.014
ecc	4.841	0.043*	0.232
loc × ecc	0.077	0.785	0.005

2-way (location loc × ecc) repeated measures ANOVA on RPF $\bar{P}_2$

RPF $\bar{P}_2$			
Within-subjects effects	$F(1,16)$	p	η_p^2
loc	0.048	0.829	0.003
ecc	5.526	0.032*	0.257
loc × ecc	9.835×10^{-5}	0.992	6.147×10^{-6}

2-way (location loc × ecc) repeated measures ANOVA on luminance decision zlog(RT)

Reaction Time (zlogRT) for luminance comparison decision			
Within-subjects effects	$F(1,16)$	p	η_p^2
loc	0.018	0.895	0.001
ecc	24.829	<0.001*	0.608
loc × ecc	1.128	0.304	0.066

2-way (location loc × ecc) repeated measures ANOVA on confidence rating zlog(RT)

Reaction Time (zlogRT) for confidence rating			
Within-subjects effects	$F(1,16)$	p	η_p^2
loc	0.715	0.399	0.045
ecc	1.051	0.321	0.062
loc × ecc	0.827	0.377	0.049

CHAPTER 3

THE GEOMETRY OF PERCEPTUAL CONFIDENCE

3.1 ABSTRACT

Visual performance can be characterized not only by the accuracy of perceptual decisions, but also by the time required to reach them. Here, we extend the relative psychometric function framework to characterize confidence jointly as a function of accuracy and response speed. Using data from an orientation-discrimination task measured across 24 visual field locations, we first show that response speed predicts confidence beyond accuracy alone. We then constructed confidence surfaces over a shared accuracy-speed domain and introduced normalized volume under the surface (nVUS), a summary measure of predicted confidence across this domain. Confidence increased independently with both accuracy and response speed. Across the visual field, eccentricity selectively altered the relationship between accuracy and confidence, which was steeper at the largest eccentricity, whereas the relationship between response speed and confidence remained stable. In contrast, neither relationship varied reliably across polar angle. nVUS was similarly elevated at the largest eccentricity but did not vary reliably across polar angle. These results demonstrate that accuracy alone provides an incomplete characterization of the objective behavior associated with perceptual confidence. More broadly, extending relative-function methods to multidimensional behavioral domains provides a flexible framework for characterizing relationships among multiple measures and a new empirical target for theories of confidence.

3.2 INTRODUCTION

Visual performance varies across the visual field not only in accuracy, but also in its temporal dynamics. At isoeccentric locations, the speed of information accrual is faster along the horizontal meridian, intermediate at intercardinal locations, slower along the lower vertical meridian, and slowest along the upper vertical meridian (Carrasco et al., 2004). When processing speed is measured independently of discriminability using speed-accuracy trade-off procedures, information processing has been found to be faster at greater eccentricities (Carrasco et al., 2003), such that more peripheral stimuli can be perceived earlier than more central stimuli (Jovanovic and Mamassian, 2019, 2020; Upadhyayula et al., 2023). These temporal differences may reflect, in part, differences in the spatiotemporal characteristics of the magnocellular and parvocellular pathways that preferentially process information from the peripheral and central visual field, respectively (Schmolesky et al., 1998). Thus, perceptual decisions that yield similar levels of accuracy need not be equivalent in the time required to reach them. Characterizing objective performance solely in terms of accuracy may therefore omit another behaviorally meaningful dimension of the decision.

Response time is also closely related to confidence. Observers tend to report greater confidence for faster perceptual decisions (Baranski and Petrusic, 1994; Fetsch et al., 2014; Kiani et al., 2014), and response time can provide information about confidence beyond that conveyed by accuracy alone (Pleskac and Busemeyer, 2010; Weidemann and Kahana, 2016). Response time has consequently also been proposed as a behavioral proxy for confidence (Miyoshi and Sakamoto, 2025). Bounded evidence-accumulation models provide one account of this relationship, in which decision uncertainty depends jointly on the state of accumulated evidence and elapsed decision time (Fetsch et al., 2014; Kiani et al., 2014; Kiani and Shadlen, 2009, see also Gold and Shadlen, 2007; Shadlen and Kiani, 2013 for reviews). Confidence may therefore be better characterized as a joint function of accuracy and decision speed than as a function of accuracy alone.

This distinction is particularly relevant to the study of subjective inflation. Subjective inflation is inherently relational: subjective reports are considered inflated insofar as they are elevated relative to objective performance. Accordingly, previous studies have typically compared confidence or other subjective measures while controlling or matching objective performance, most commonly using detection

or discrimination accuracy or perceptual sensitivity. Similarly, relative psychometric functions (RPFs) characterize subjective reports conditional on objective performance across a range of performance levels, rather than subjective reports in isolation (Maniscalco et al., 2026; Shen and Peters, 2026; Tian et al., 2025). However, matching accuracy equates one outcome of a perceptual decision; it does not necessarily equate the decision itself. In particular, two conditions matched in accuracy may differ systematically in the time required to reach those decisions. Apparent differences in confidence at matched accuracy could therefore occur alongside systematic differences in the temporal dynamics of the decisions being compared.

To our knowledge, previous studies have not systematically assessed the entire quantitative relationship between objective and subjective performance while jointly accounting for both accuracy and response time. Accounting for the temporal dimension of perceptual decisions may also constrain mechanistic explanations of subjective inflation. Whereas prominent accounts propose that inflation can result from applying a common criterion to representations that differ in uncertainty (Morales et al., 2015; Rahnev et al., 2011), other work suggests that decision and confidence boundaries can themselves vary as a function of uncertainty (Adler and Ma, 2018; Denison et al., 2018). Differences in confidence may therefore reflect not only differences in the quality of sensory representations, but also differences in how evidence is accumulated or mapped onto perceptual decisions and confidence.

The preceding chapters provide converging reasons to consider this additional dimension of perceptual behavior. In Chapter 1, we examined whether spatial differences in objective performance, operationalized using task accuracy or perceptual sensitivity, correspond to spatial differences in metacognition. The relationship between confidence and performance was relatively invariant across much of the visual field, leading us to consider whether subjective inflation might depend on contextual changes in sensory uncertainty rather than stable differences between visual field locations. In Chapter 2, we manipulated physical noise directly using a temporally evolving brightness-comparison task. We found some evidence consistent with subjective inflation, together with systematic differences in response time: observers responded faster parafoveally than peripherally, with suggestive evidence that this difference varied with stimulus noise. Together, these findings raise the possibility that accuracy alone provides an incomplete description of the objective behavior against which confidence is evaluated.

The response time data from Chapter 1 provides a useful basis for examining this possibility. Response times decreased systematically with increasing stimulus contrast, consistent with faster decisions as

perceptual evidence increased. This relationship was evident across eccentricities and polar angles **(Figure 3.1)**. Thus, the same dataset used to characterize the relationship between accuracy and confidence contains systematic variation in a second dimension of perceptual behavior: the time required to reach the decision.

Here, we revisit these data to characterize confidence jointly as a function of accuracy and response speed. We first ask whether response speed predicts confidence after accounting for accuracy. We then extend the RPF approach from a relationship between confidence and a single objective dimension, $C = f(A)$ to a surface relating confidence jointly to accuracy and response speed, $C = f(A, S)$. Finally, we ask whether this joint relationship varied systematically with eccentricity and polar angle. This approach allows us to characterize not simply whether confidence differs across conditions, but whether the mapping between confidence and multiple dimensions of objective perceptual behavior differs across the visual field.

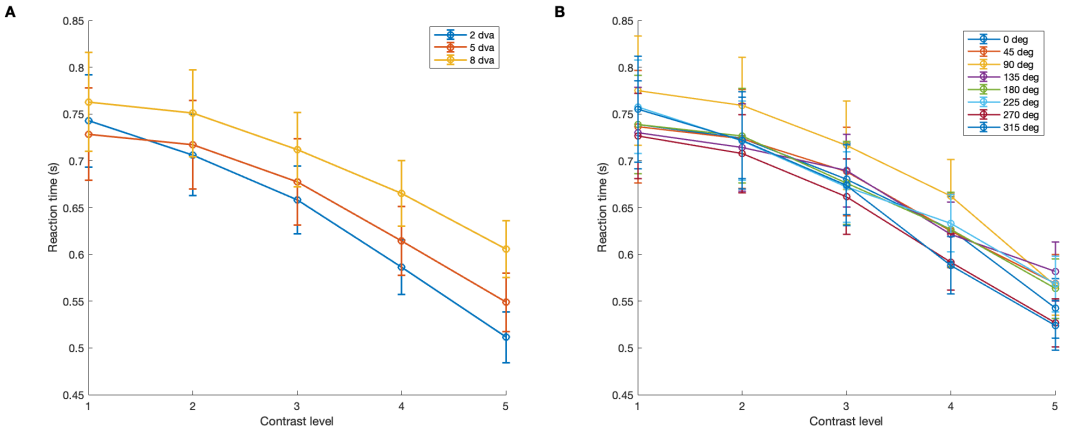

Figure 3.1: **Reaction time as a function of stimulus contrast and visual field location.** Mean reaction times are shown across the five contrast levels, separately by (A) eccentricity and (B) polar angle. Points indicate group means and error bars represent ±1 SEM. Reaction times decreased with increasing stimulus contrast. Responses were generally slower at greater eccentricities and varied across polar angle locations.

3.3 METHODS

3.3.1 Data preprocessing and construction of accuracy-speed trajectories

Throughout the following analyses, we used linear interpolation between observed data points rather than assuming a parametric form for the underlying relationships. This nonparametric approach follows the interpolation-based framework introduced for relative psychometric functions (RPFs; Maniscalco et al., 2026).

Response time (RT) was defined as the interval between the onset of the response cue and the observer's keypress. Observers were required to respond within a 2000 ms response window. Because the response cue occurred at a fixed delay following stimulus offset on every trial, response cue-referenced and stimulus-referenced RTs differed only by a constant offset. RTs were log-transformed and standardized separately within each observer, and the sign of the resulting z-scores were inverted so that larger values indicated faster responses:

$$S = -z_i \log(RT) \tag{3.1}$$

where S denotes response speed and the z-transformation was performed separately within each observer.

For each observer and stimulus location, trials were pooled within each of the five stimulus-contrast levels to obtain mean accuracy, confidence, and response speed. Because expected accuracy in a two-alternative forced-choice task is bounded below by chance and is expected to increase monotonically with stimulus contrast, observed accuracy estimates were constrained to the interval [.5 1] and subjected to isotonic regression across increasing contrast. Specifically, the fitted accuracy estimates A_k^* were constrained such that:

$$.5 \leq A_1^* \leq A_2^* \leq A_3^* \leq A_4^* \leq A_5^* \leq 1 \tag{3.2}$$

where k indexes increasing stimulus-contrast level. The isotonic solution was obtained using the pool-adjacent-violators algorithm (PAVA), providing a minimally constrained estimate of the underlying performance trajectory while reducing reversals attributable to finite sampling.

When PAVA pooled adjacent contrast levels, the resulting levels had identical fitted accuracy values. Because subsequent analyses required unique coordinates in accuracy-speed space, tied levels were collapsed into a single trajectory vertex. Accuracy, confidence, and response speed were averaged across the corresponding pooled levels. Each observer-by-location condition was therefore represented by a sequence of between two and five unique vertices (A, S, C), describing the observed trajectory through accuracy-speed-confidence space as stimulus contrast increased. Conditions yielding fewer than three unique vertices were excluded from subsequent analyses. Two conditions met this exclusion criterion, leaving 358 observer-by-location trajectories for analysis (15 observers × 24 locations, minus two excluded conditions). Retained trajectories therefore contained between three and five unique vertices.

For mixed-effects modeling, accuracy was linearly rescaled from its task-relevant range of [.5, 1] to [0, 1] and then grand-mean centered, $A_c = A - \bar{A}$. Response speed, already expressed in within-observer standard deviation units by the transformation above, was likewise grand-mean centered before model fitting. Centering allowed model intercepts and lower-order effects to be interpreted at the average value of the other continuous predictor while preserving the original two-dimensional geometry of accuracy and response speed.

3.3.2 Modeling confidence as a joint function of accuracy and response speed

We next asked whether confidence could be characterized as a joint function of objective accuracy and response speed, such that:

$$C = f(A, S) \tag{3.3}$$

where C denotes confidence, A denotes accuracy, and S denotes response speed. Whereas the analyses in Chapter 1 characterized confidence as a function of accuracy alone, this analysis tested whether response speed contained additional information associated with confidence after accounting for accuracy, and whether the mappings between accuracy, response speed, and confidence varied across the visual field.

Because neither accuracy nor response speed was manipulated independently, the observed data did not densely sample the two-dimensional accuracy-by-speed domain required to estimate an empirical confidence surface directly. Instead, increasing stimulus contrast generated a sequence of jointly varying

accuracy, response speed, and confidence values at each visual field location. We therefore represented each location as a trajectory through three-dimensional (A, S, C) space:

$$c \longmapsto (A(c), S(c), C(c)) \tag{3.4}$$

where c indexes stimulus contrast.

We first examined these trajectories to determine whether variation in response speed was largely redundant with variation in accuracy. There was substantial variation in response speed among observations with similar accuracy (see **Figure 3.2**), motivating an explicit test of whether response speed explained confidence beyond accuracy.

We therefore tested the independent contributions of accuracy and response speed to confidence using linear mixed-effects models. Preliminary models successively predicted confidence from accuracy alone,

$$M_0: \quad C \sim A_c + (1 \mid \text{observer}) \tag{3.5}$$

additive effects of accuracy and response speed,

$$M_1: \quad C \sim A_c + S_c + (1 \mid \text{observer}) \tag{3.6}$$

and their interaction,

$$M_2: \quad C \sim A_c * S_c + (1 \mid \text{observer}). \tag{3.7}$$

Model fit improved with the addition of response speed (M_0: AIC = 1050.25, BIC = 1071.46; M_1: AIC = 882.58, BIC = 909.09) and further improved with the accuracy-by-speed interaction (M_2: AIC = 842.06, BIC = 873.88). We therefore retained both predictors and their interaction in subsequent models.

We next expanded the random-effects structure to account for repeated observations within visual-field locations and observer-specific relationships between the continuous predictors and confidence. Model comparisons favored inclusion of both location-within-observer intercepts (AIC = 737.81, BIC = 774.92) and observer-specific slopes (AIC = 315.30, BIC = 378.94). Allowing the accuracy-by-speed interactions to additionally vary across observers further improved model fit (AIC = 269.84, BIC = 354.69).

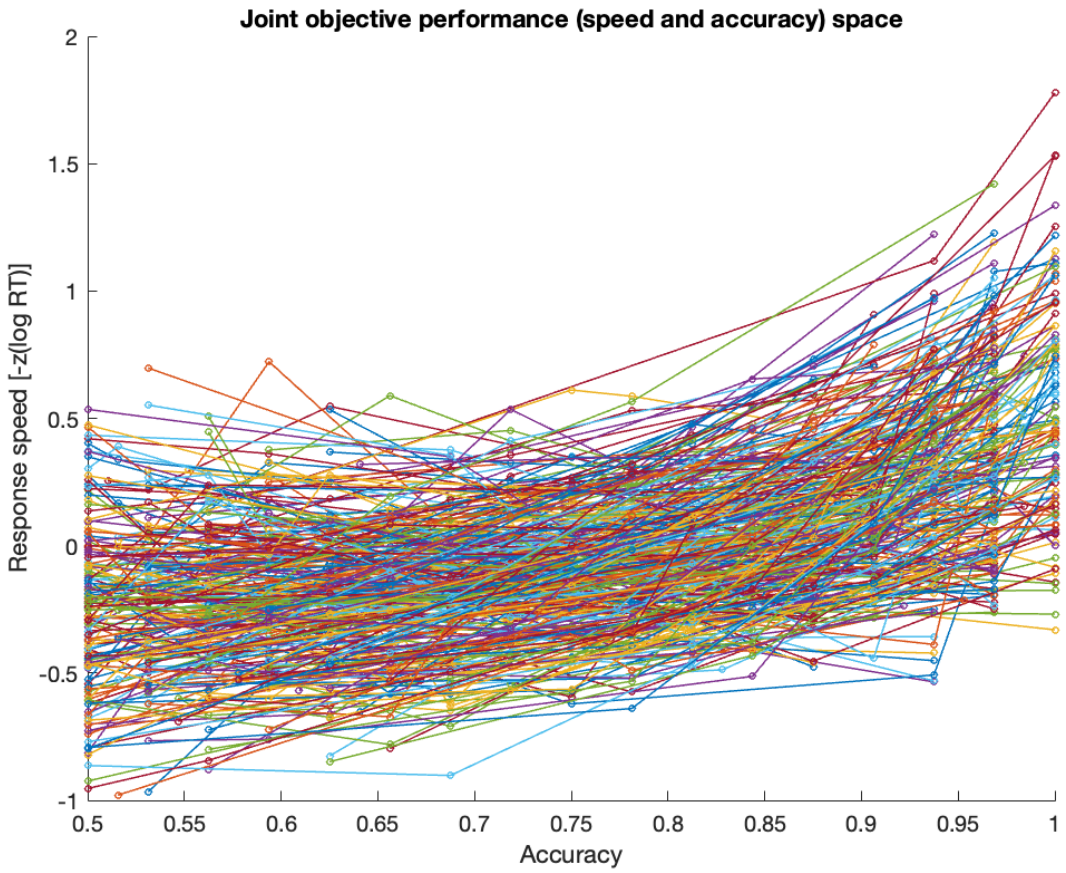

Figure 3.2: **Joint distribution of accuracy and response speed.** Standardized response speed is plotted against accuracy for each observer and visual field location, with points connected across contrast levels within each observer-by-location trajectory. Response speed was defined as the negative standardized log transformed reaction time, such that higher values indicate faster responses. Substantial variation in response speed was evident among observations with similar accuracy, demonstrating that accuracy and response speed provided partially distinct information about objective performance.

These comparisons motivated the primary model:

$$M_{\text{full}}: \quad C \sim A_c * S_c + (1 + A_c * S_c \mid \text{observer}) + (1 \mid \text{observer} : \text{location}) \tag{3.8}$$

which included fixed effects of centered accuracy A_c, centered response speed S_c, and their interaction; observer-specific random intercepts and slopes for each of these terms; and a random intercept for visual field location nested within observer.

To test whether the mappings from accuracy and response speed to confidence varied with eccen-

tricity, we fit:

$$M_{\text{ecc}}: \quad C \sim A_c * \text{ecc} + S_c * \text{ecc} + A_c : S_c + (1 + A_c * S_c \mid \text{observer}) + (1 \mid \text{observer} : \text{location}) \tag{3.9}$$

This model allowed both the accuracy-confidence and speed-confidence relationships to vary across eccentricities while retaining the accuracy-by-speed term from the primary model.

An analogous model tested variation across polar angle:

$$M_{\text{angle}}: \quad C \sim A_c * \text{angle} + S_c * \text{angle} + A_c : S_c + (1 + A_c * S_c \mid \text{observer}) + (1 \mid \text{observer} : \text{location}) \tag{3.10}$$

3.3.3 Construction of the empirical confidence surface

To characterize confidence jointly as a function of accuracy and response speed, we constructed observer- and location-specific confidence surfaces, $C_{ij}(A, S)$, where i indexes observers and j indexes visual-field locations. Because accuracy and response speed were correlated, and some combinations of the two variables were therefore sparsely or not empirically supported, surfaces were evaluated only over observer-specific regions of the accuracy-speed space.

For each observer, we first defined an empirical accuracy-speed domain, $\mathcal{D}_i$, pooling observations across all retained visual-field locations (see **Figure 3.3**). At accuracy values between .5 and 1 in increments of .01, we identified observations falling within a local accuracy window of ±.075. Where there were at least 10 observations available within the window, the lower and upper speed boundaries were defined as the 5th and 95th percentiles, respectively, of the local speed distribution. This procedure yielded a continuous central 90% envelope of empirically supported response speeds across accuracy (**Figure 3.4**). The resulting domain was shared across all retained locations for a given observer, ensuring that location-specific confidence surfaces were compared over the same accuracy-speed region.

For numerical evaluation, the boundaries of $\mathcal{D}_i$ were linearly interpolated onto a fine grid and the enclosed region was partitioned into equal-area cells using midpoint intervals of $\Delta A = .005$ and $\Delta S = .01$. The area of the observer-specific domain was therefore approximated as:

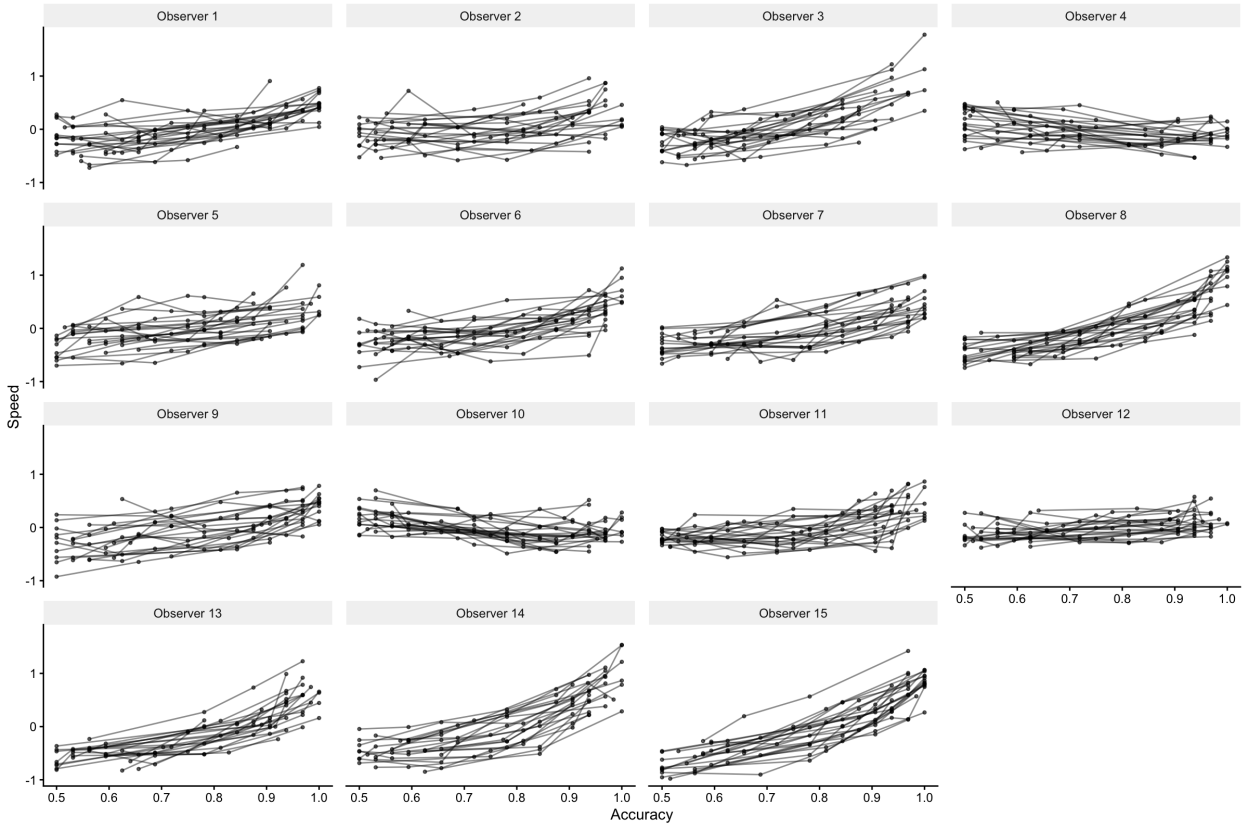

Figure 3.3: **Observer-level accuracy-speed trajectories across visual field locations.** Accuracy is plotted against standardized response speed separately for each observer. Within each panel, lines show the accuracy-speed trajectories for the 24 visual field locations, obtained across contrast levels after isotonic regression and pooling of adjacent accuracy levels.

$$\mathcal{D}_i \approx N_i \Delta A \Delta S \tag{3.11}$$

where N_i is the number of grid cells falling within the domain.

The fitted accuracy-speed model was then evaluated at each grid point separately for every retained observer and visual field location. Predictions included all fitted random effects, such that each surface incorporated the observer-specific random intercept and slopes for accuracy, speed, and their interaction, as well as the observer-by-location random intercept. Thus, $C_{ij}(A, S)$ represented the fitted confidence surface evaluated throughout the common observer-specific domain $\mathcal{D}_i$.

We summarized each surface by numerically integrating predicted confidence over its accuracy-speed domain. Using midpoint Riemann integration, the volume under the surface (VUS) was approximated as:

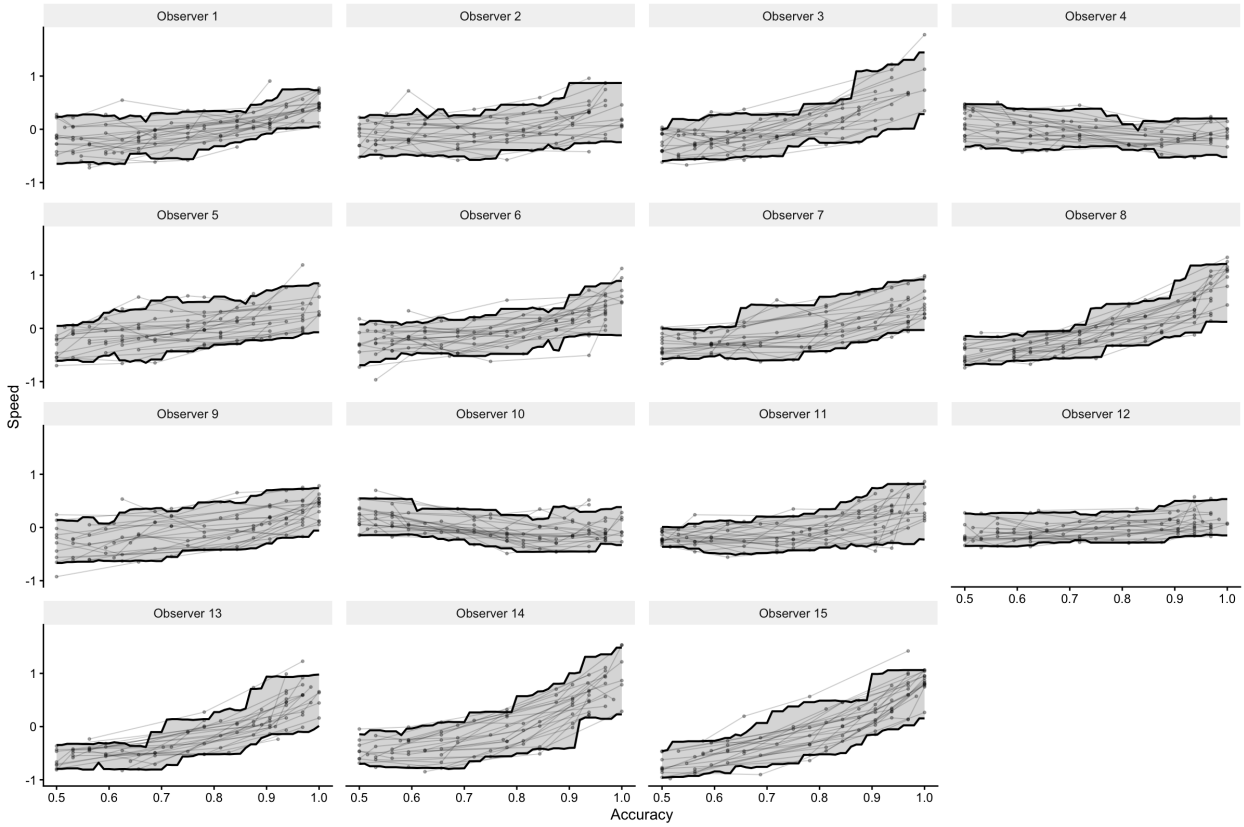

Figure 3.4: **Observer-level empirical support in accuracy-speed space.** Accuracy-speed trajectories are shown separately for each observer and visual field location. Black outlines indicate the observer-specific region of empirical support used for subsequent surface estimation, defined from the central 90% of the observed response-speed distribution across accuracy. Only accuracy-speed combinations within these supported regions were used in subsequent analyses.

$$\mathrm{VUS}_{ij} = \iint_{\mathcal{D}_i} C_{ij}(A,S)\,\mathrm{d}A\,\mathrm{d}S \approx \sum_{k=1}^{N_i} C_{ij}(A_k,S_k)\Delta A \Delta S \tag{3.12}$$

Because the size of the empirically supported accuracy-speed domain differed across observers, VUS was normalized by the corresponding domain area:

$$\mathrm{nVUS}_{ij} = \frac{VUS_{ij}}{|\mathcal{D}_i|} = \frac{\iint_{\mathcal{D}_i} C_{ij}(A,S)\,\mathrm{d}A\,\mathrm{d}S}{\iint_{\mathcal{D}_i} 1\,\mathrm{d}A\,\mathrm{d}S} \tag{3.13}$$

We refer to this quantity as normalized volume under the surface (nVUS). Because all integration cells had equal area, nVUS is equivalently the mean predicted confidence across the observer's supported accuracy-speed domain and therefore remains on the original confidence-rating scale. Using a common

domain across locations within each observer ensured that the differences in nVUS across visual-field conditions reflected differences in the fitted confidence surfaces rather than differences in the accuracy-speed regions over which they were evaluated.

More complex mixed-effects models allowing observer-specific random effects of both eccentricity and polar angle produced singular fits and were therefore not interpreted. Spatial variation in nVUS was consequently assessed using the marginal within-observer analyses described below.

3.3.4 Eccentricity-specific confidence surfaces and nVUS

To characterize how the joint relationship between accuracy, response speed, and confidence varied with eccentricity, the fitted eccentricity model was evaluated separately at each retained visual-field location over the observer-specific accuracy–speed domain, $\mathcal{D}_i$. Each resulting location-specific confidence surface was integrated and normalized by the area of $\mathcal{D}_i$ to obtain nVUS_{ij}. Location-specific nVUS values were then averaged across polar angle within each eccentricity to obtain one value per observer at 2, 5, and 8 dva.

Differences in nVUS across eccentricities were then assessed using a one-way repeated-measures ANOVA. Degrees of freedom were Greenhouse-Geisser corrected where the assumption of sphericity was violated, and significant effects were followed by Tukey-adjusted pairwise comparisons.

3.3.5 Polar angle-specific confidence surfaces and nVUS

To characterize how the joint relationship between accuracy, response speed, and confidence varied with polar angle, the fitted polar-angle model was evaluated separately at each retained visual field location over the observer-specific accuracy-speed domain, $\mathcal{D}_i$. Each resulting location-specific confidence surface was integrated and normalized by the area of $\mathcal{D}_i$ to obtain nVUS_{ij}. Location-specific nVUS were then averaged across eccentricity within each polar angle to obtain one value per observer at each of the eight polar angles. Differences in nVUS across polar angles were assessed using a one-way repeated-measures ANOVA, with Greenhouse-Geisser-corrected degrees of freedom where appropriate.

3.3.6 Statistical analysis

Statistical analyses were performed in R (v4.6.1). Linear mixed-effects models were fit using the lme4 (Bates et al., 2015), lmerTest (Kuznetsova et al., 2017), and afex (Singmann et al., 2025) packages. Nested models were compared using maximum-likelihood estimation, whereas final mixed-effects models were fit using restricted maximum likelihood (REML), with Type III tests and Kenward-Roger approximations for denominator degrees of freedom. Significant effects were followed by pairwise comparisons of estimated marginal means with Tukey adjustment for multiple comparisons using the emmeans package (Lenth and Piaskowski, 2026). Repeated measures analyses of nVUS were conducted using afex, with Greenhouse-Geisser corrections applied where appropriate. Partial η^2, calculated using the effectsize package (Ben-Shachar et al., 2020), is reported as a measure of effect size.

3.4 Results

3.4.1 Preprocessing results

After exclusion of the two observer-by-location conditions with fewer than three (A, S, C) vertices, 151 of 358 accuracy trajectories (42.2%) contained at least one empirical decrease in accuracy with increasing contrast. These decreases were generally small (median largest decrease = 0.063), consistent with sampling variability around an underlying monotonic psychometric function. Following bounded isotonic regression and pooling of tied vertices, 53 (14.80%) contained three unique vertices, 199 (55.59%) contained four, and 106 (29.61%) retained all five.

3.4.2 Confidence as a joint function of accuracy and response speed

Accuracy and response speed independently predict confidence

In the primary model, confidence increased strongly with accuracy (F(1,13.89)=200.37, p<.001, β=1.33, SE=.09) and also with response speed (F(1,13.93)=48.25, p<.001, β=.38, SE=.05). Thus, faster responses were associated with greater confidence even after accounting for accuracy. There was no evidence for a consistent population-level interaction between accuracy and response speed (F(1,13.87)=1.62, p=.225,

β=.18, SE=.14). However, the subject-level standard deviation of the accuracy-by-speed interaction slope was .46, indicating substantial individual variability in how accuracy and response speed jointly related to confidence.

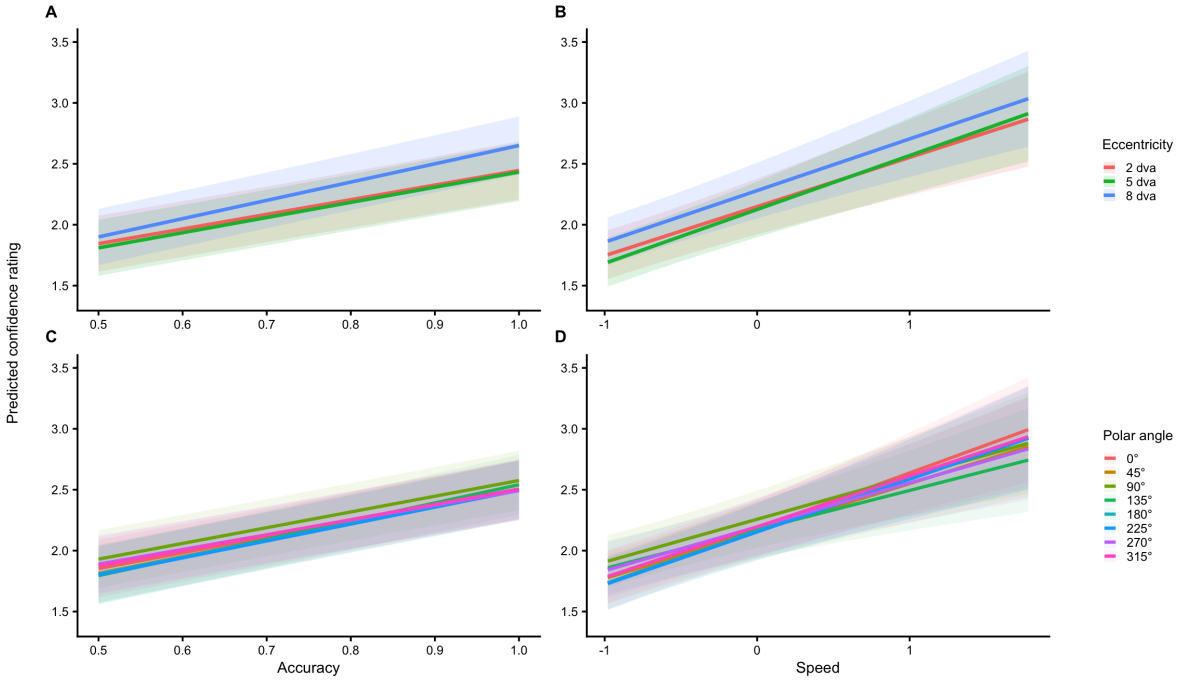

Figure 3.5: **Model-predicted confidence as a function of accuracy and response speed across visual field locations.** Predicted confidence ratings are shown as a function of (A) accuracy across eccentricities, (B) response speed across eccentricities, (C) accuracy across polar angles, and (D) response speed across polar angles. Predictions for accuracy were evaluated at mean response speed, and predictions for response speed were evaluated at mean accuracy. Shaded regions indicate 95% confidence intervals. Confidence increased with both accuracy and response speed. The accuracy-confidence relationship was steeper at 8 dva than at 2 or 5 dva, whereas the speed-confidence relationship did not differ across eccentricities. Neither relationship differed reliably across polar angles.

Eccentricity selectively alters the accuracy-confidence relationship

We next tested whether the relationships between accuracy, response speed, and confidence varied with eccentricity. Adding eccentricity and its interactions substantially improved model fit relative to the primary model ($\chi^2(6)=95.97$, $p<.001$), and was favored by both AIC (185.87 vs. 269.84) and BIC (302.54 vs. 354.69).

Confidence varied significantly with eccentricity after accounting for accuracy and response speed ($F(2,353.53)=21.51$, $p<.001$). At mean accuracy and response speed, estimated marginal confidence was

2.15 at 2 dva, 2.13 at 5 dva, and 2.28 at 8 dva. Critically, the relationship between accuracy and confidence also varied with eccentricity (F(2,1268.51)=19.04, p<.001; **Figure 3.5A**). Estimated accuracy-confidence slopes were 1.20 at 2 dva, 1.25 at 5 dva, and 1.50 at 8 dva. Tukey-adjusted comparisons indicated that the slopes did not differ between 2 and 5 dva (p=.697), whereas the slope at 8 dva was significantly steeper than at both 2 and at 5 dva (both p<.001).

In contrast, the relationship between response speed and confidence did not vary with eccentricity, (F(2,1393.97)=0.30, p=.744; **Figure 3.5B**). Estimated speed-confidence slopes were highly similar across eccentricities (.40, .44, and .42 at 2, 5, and 8 dva, respectively). The accuracy-by-speed interaction was also not significant (F(1,14.15)=3.58, p=.079). Thus, eccentricity altered both overall confidence and the mapping between accuracy and confidence, but there was no evidence that it altered the mapping between response speed and confidence.

Accuracy-confidence and speed-confidence relationships are stable across polar angle

Finally, we tested whether these relationships varied across polar angle. The expanded polar angle model produced a modest improvement in log likelihood relative to the primary model (χ^2(21)=36.52, p=.019) but the additional complexity was not favored by information criteria (AIC = 275.32 vs. 269.84; BIC = 471.54 vs. 354.69).

After accounting for accuracy and response speed, confidence did not vary significantly with polar angle (F(7,339.63)=1.20, p=.300). There was also no significant evidence that the accuracy-confidence relationship varied across polar angle (F(7,1220.28)=1.76, p=.092; **Figure 3.5C**), or that the speed-confidence relationship varied across polar angle (F(7,1336.23)=0.62, p=.743; **Figure 3.5D**). The accuracy-by-speed interaction was also not significant (F(1,13.90)=1.31, p=.272).

Together, these results show that response speed explained variation in confidence beyond that captured by accuracy, but its relationship with confidence was stable across both eccentricity and polar angle. Spatial variation was instead specific to the accuracy-confidence relationship: this mapping was stable across polar angle but became steeper at the largest eccentricity.

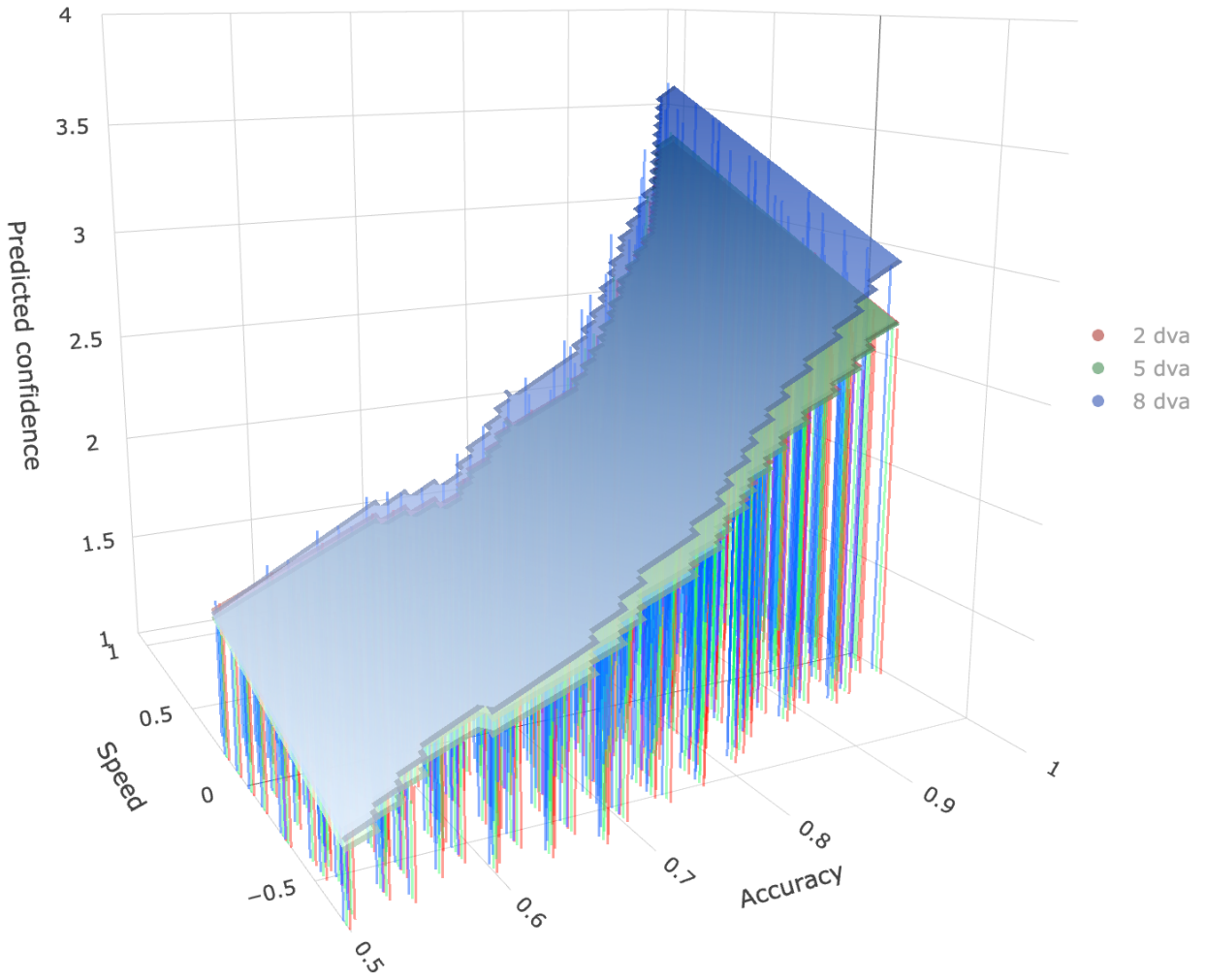

Figure 3.6: **Predicted confidence as a joint function of accuracy and response speed across eccentricities.** Surfaces show model-predicted confidence, $C = f(A, S)$, across the empirically supported accuracy-speed domain for each eccentricity (2, 5, and 8 dva). Vertical lines extend from the minimum confidence rating (1) to the predicted surface and illustrate the volume under each surface. For visualization only, vertical columns were slightly offset along the speed axis to distinguish overlapping conditions; no such offset was applied in the calculation of nVUS.

3.4.3 Confidence surfaces across eccentricity

The eccentricity-specific confidence surfaces reflected the previously observed modulation of the relationship between accuracy and confidence by eccentricity (**Figure 3.6**). Consistent with the two-dimensional model predictions above **(Figure 3.5A,B)**, the eccentricity-specific confidence surfaces diverged primarily along the accuracy dimension: the 8 dva surface increased more steeply with accuracy than the 2 and 5

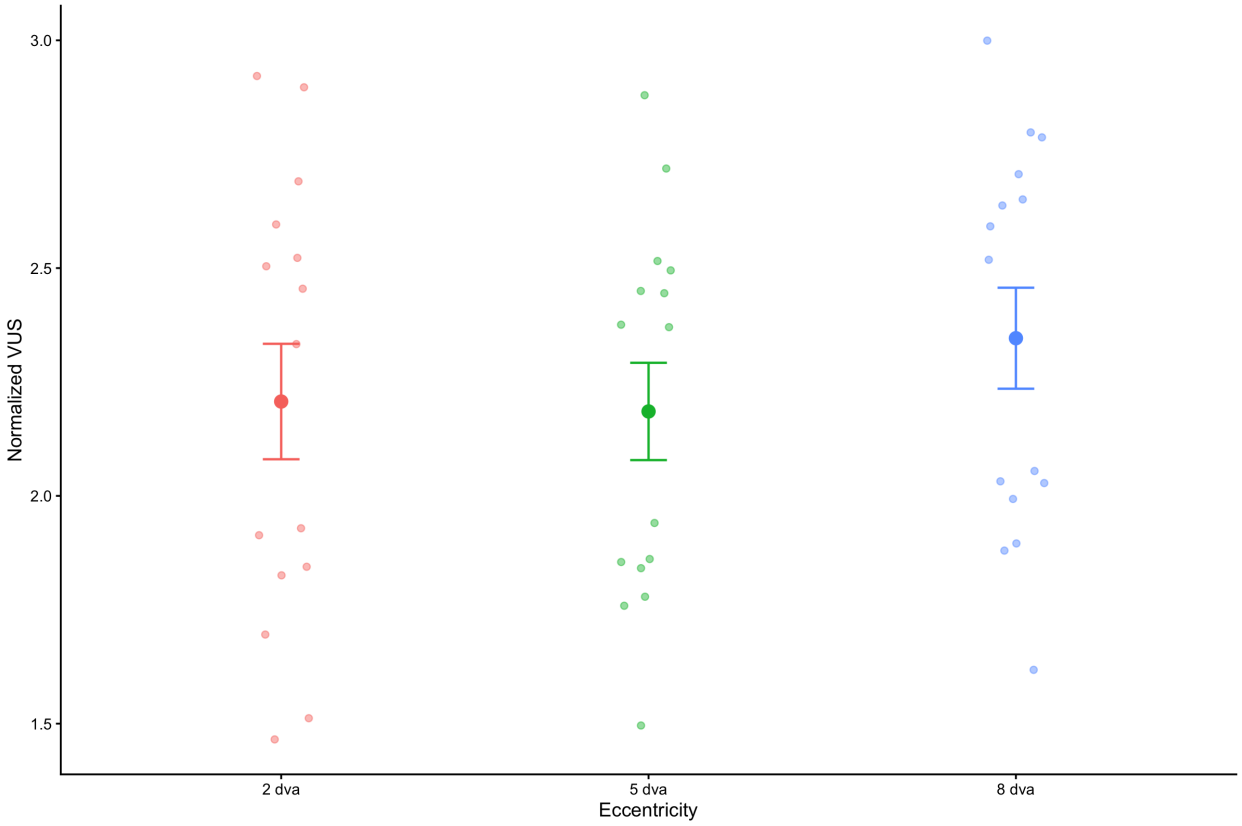

Figure 3.7: **Normalized volume under the surface (nVUS) across eccentricity.** Small points show individual observer nVUS values at each eccentricity. Large points indicate group means, with error bars representing ±1 SEM. nVUS differed significantly across eccentricities, with higher values at 8 dva than at 2 and 5 dva, which did not differ from one another.

dva surfaces, whereas their gradients along the response-speed dimension were similar.

Mean nVUS also differed across eccentricities ($F(1.23,17.21)=10.47$, $p=.003$, $\eta_p^2=.428$). Mean nVUS was 2.21 at 2 dva, 2.19 at 5 dva, and 2.35 at 8 dva (**Figure 3.7**). Tukey-adjusted pairwise comparisons indicated that nVUS was greater at 8 dva than at both 2 dva ($p=.028$) and 5 dva ($p<.001$), whereas 2 and 5 dva did not differ ($p=.863$). Thus, after jointly accounting for accuracy and response speed over a common observer-specific domain, predicted confidence was elevated at the largest eccentricity.

3.4.4 Confidence surfaces across polar angle

Consistent with the two-dimensional model predictions above **(Figure 3.5C,D)**, the polar angle-specific confidence surfaces were broadly similar in their dependence on accuracy and response speed (**Figure**

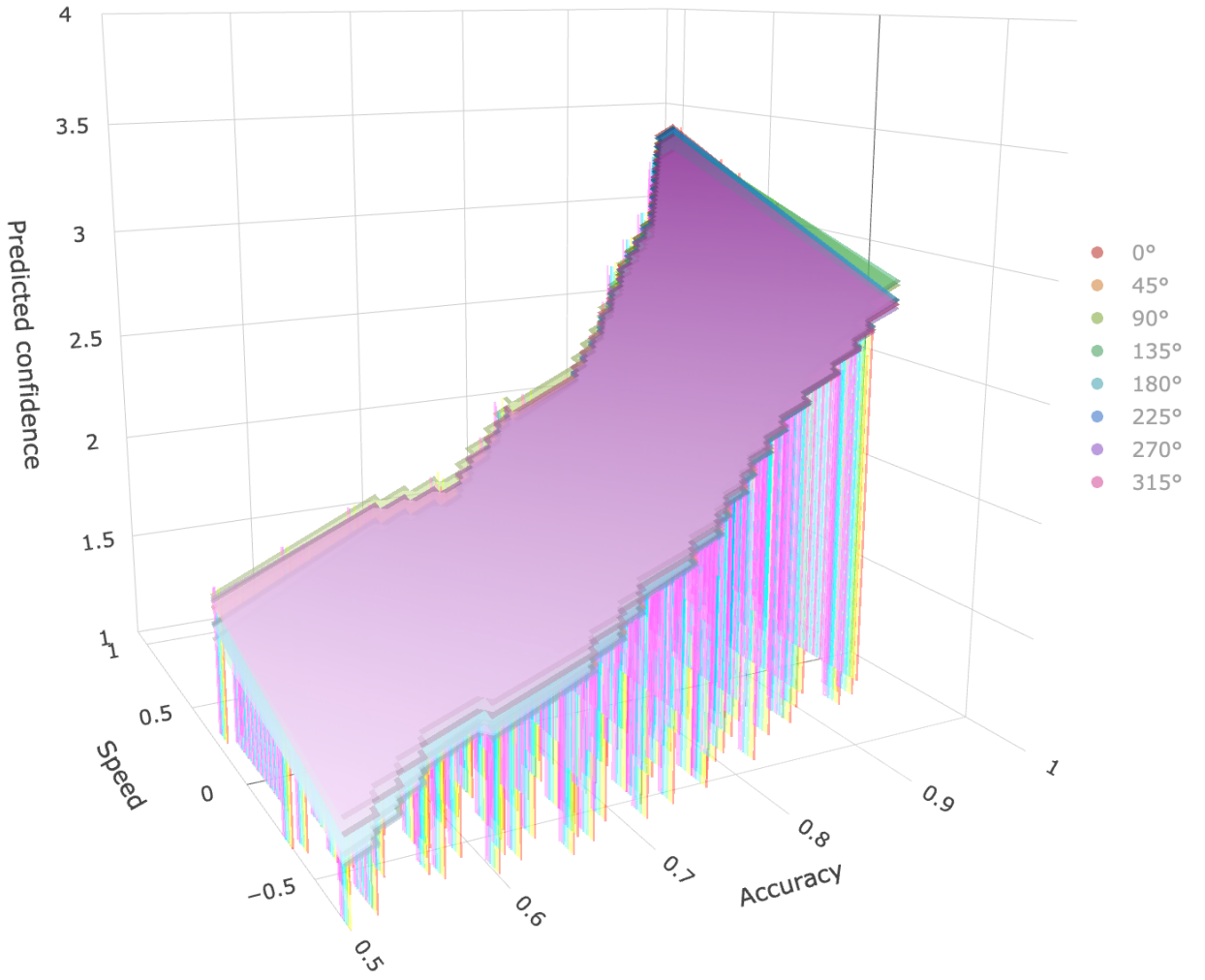

Figure 3.8: **Predicted confidence as a joint function of accuracy and response speed across polar angles.** Surfaces show model-predicted confidence, $C = f(A, S)$, across the empirically supported accuracy-speed domain for each polar angle (0° to 315° in 45° increments). Vertical lines extend from the minimum confidence rating (1) to the predicted surface and illustrate the volume under each surface.

3.8).

Mean nVUS did not significantly differ across polar angles (F(4.13,57.77)=2.04, p=.099, η_p^2=.127). Mean nVUS ranged from 2.21 to 2.31 across eight polar angles (**Figure 3.9**). Thus, unlike eccentricity, we found no evidence that polar angle reliably modulated mean predicted confidence over the joint accuracy-speed domain.

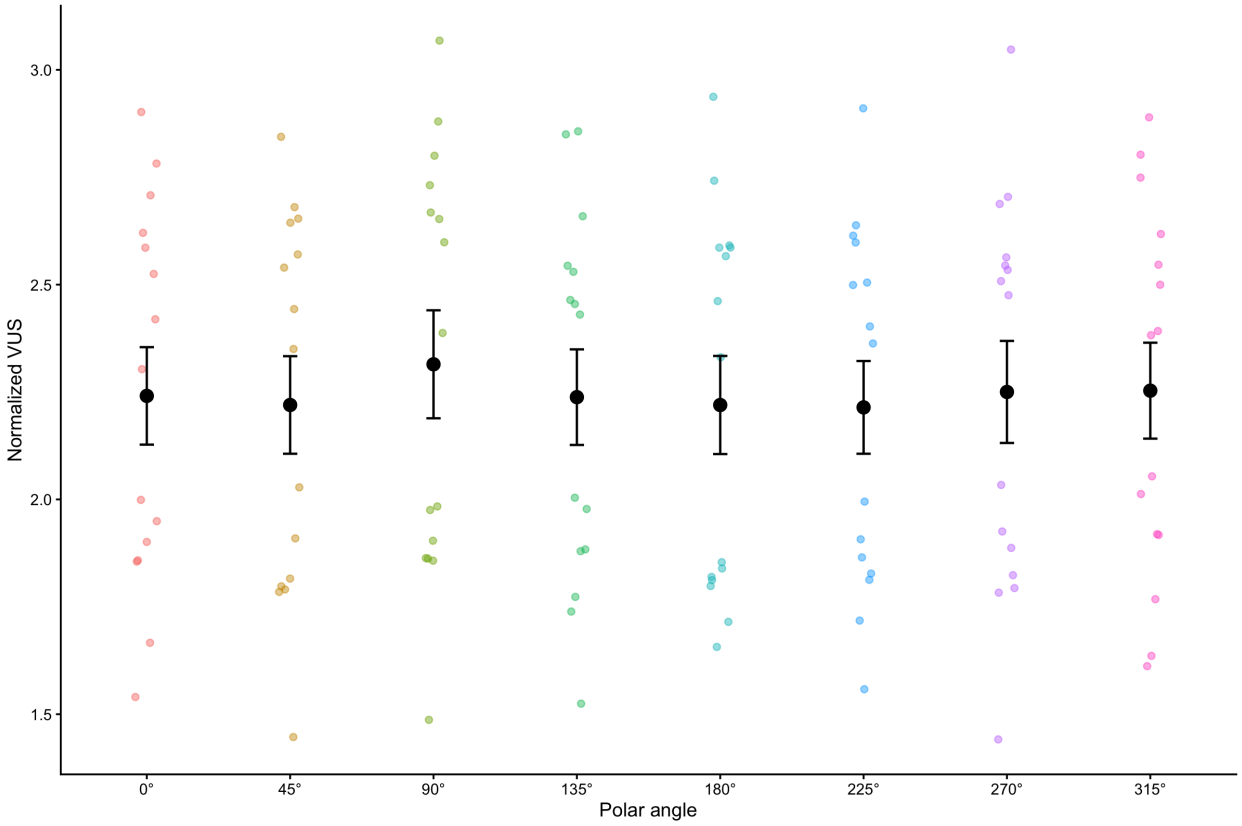

Figure 3.9: **Normalized volume under the surface (nVUS) across polar angle.** Small points show individual observer nVUS values at each polar angle. Large points indicate group means, with error bars representing ±1 SEM. nVUS did not differ significantly across polar angle.

3.5 Discussion

Perceptual confidence is closely related to objective performance, but accuracy alone provides an incomplete description of perceptual behavior. Here, we asked how confidence relates jointly to the accuracy and speed of perceptual decisions, and whether this relationship changes across the visual field. Confidence depended on both accuracy and response speed, but spatial variation was selective: the accuracy-confidence relationship varied with eccentricity, whereas the response-speed relationship remained relatively stable across both eccentricity and polar angle.

We first established that accuracy and response speed jointly predict confidence. Across observers and stimulus locations, confidence increased with both accuracy and response speed, with each explaining variance beyond the other. Thus, accuracy alone does not fully characterize the behavioral

variation associated with confidence. This is particularly important given the longstanding recognition that response speed and accuracy jointly characterize decision performance (Christie and Luce, 1956; Henmon, 1911; Wickelgren, 1977).

We next asked whether these relationships varied across the visual field. Eccentricity selectively altered the accuracy–confidence relationship, which was steeper at the largest eccentricity, where confidence was also higher overall. In contrast, the speed–confidence relationship remained relatively stable. This pattern extends the eccentricity-dependent differences observed in Chapter 1 by showing that they persist when response speed is considered alongside accuracy. The result is also consistent with subjective inflation in peripheral vision, where subjective perceptual judgments can outstrip objective accuracy (Odegaard et al., 2018a; Rajananda et al., 2017; Solovey et al., 2015, but see Pruitt et al., 2024). Here, this apparent inflation persisted even when performance was characterized jointly by accuracy and response speed.

In contrast, we found little evidence that either component of the confidence mapping varied systematically with polar angle. This relative invariance is notable given pronounced polar-angle asymmetries in perceptual performance, including differences in the temporal dynamics of visual processing (Carrasco et al., 2004). Together with Chapter 1, these findings suggest that first-order polar-angle asymmetries do not translate straightforwardly into corresponding differences in subjective confidence, even when response speed is considered alongside accuracy.

The RPF provides a general framework for comparing two measures over a shared domain, allowing relationships between perception and metacognition to be characterized continuously rather than at a small number of matched points (Maniscalco et al., 2026). However, many psychological constructs are multidimensional, with multiple components that may jointly relate to another measure. Here, we extend the RPF framework into a third dimension, replacing a relative function with a relative surface over a shared two-dimensional domain. In the present application, this approach allowed us to compare confidence over a shared domain of accuracy and response speed for every observer, while retaining the continuous relationship among all three measures. To our knowledge, this represents the first extension of relative-function methods to characterize relationships among measures over a multidimensional shared domain.

Extending the RPF into additional dimensions also requires an analogous summary measure. Integrating the surface over the shared domain and normalizing by its area yields nVUS, which here represents

average predicted confidence across comparable accuracy-speed states. Importantly, nVUS complements rather than replaces the geometry of the surface. Component relationships identify how confidence varies along individual dimensions, while the surface captures how those dimensions jointly relate to confidence. nVUS, in turn, summarizes their overall elevation across the shared domain. Agreement among these measures therefore indicates a systematic difference in confidence across the shared domain, whereas disagreement can reveal changes in the shape or location of the relationship that are lost through integration. Two conditions may, for example, have differently shaped surfaces but similar nVUS if local differences cancel when integrated, or similar surface geometry but different nVUS if one surface is consistently elevated. In the present data, the convergence of the component-wise and nVUS analyses therefore suggests that eccentricity produces a systematic difference in confidence over the accuracy-speed domain, whereas the confidence mapping remains comparatively stable across polar angle.

The joint accuracy-speed-confidence relationship also provides a richer empirical constraint for process models of confidence. Existing accounts differ in the information assumed to underlie confidence and in how that information is transformed into a subjective judgment (Shekhar and Rahnev, 2023). Models that jointly predict choice, decision time, and confidence — particularly evidence-accumulation and post-decisional accounts (Hellmann et al., 2023; Herregods et al., 2025; Pleskac and Busemeyer, 2010) — should therefore reproduce not only the marginal relationships between confidence and accuracy or response speed, but their joint geometry. The present results provide additional spatial constraints: a successful account should explain why the accuracy-confidence relationship changes with eccentricity while the speed-confidence relationship remains relatively stable, and why both relationships are comparatively invariant across polar angle despite pronounced differences in first-order visual processing. Models that do not explicitly incorporate decision time could similarly be extended to generate predictions for this joint behavioral space. Thus, $C = f(A, S)$ provides a descriptive target against which competing accounts of the processes generating confidence can be evaluated.

3.5.1 Limitations and future directions

Our analyses also revealed substantial individual variation in the accuracy-speed-confidence relationship. Observers differed both in overall confidence across the joint behavioral domain and in how accuracy and

response speed mapped onto confidence. Indeed, allowing these relationships to vary across observers substantially changed the apparent population-level interaction between accuracy and response speed, suggesting that a single group-average surface may obscure meaningful individual differences. An important next step will be to determine whether these differences are stable characteristics of individual observers and whether they can be captured by variation in the parameters of a common process model. Applying this framework within individuals across tasks or sessions could further distinguish stable differences in confidence computation from context-dependent changes in the confidence mapping.

Several features of our three-dimensional RPF approach also delimit its interpretation. Accuracy and response speed are naturally coupled through the speed-accuracy tradeoff (Heitz, 2014), such that observers do not occupy all theoretically possible combinations of the two measures. We therefore restricted each confidence surface to the empirically supported accuracy-speed domain rather than extrapolating into unobserved behavioral states. Consequently, $C = f(A, S)$ describes the joint structure of accuracy, response speed, and confidence but does not establish causal contributions of either behavioral measure to confidence. Future experiments could independently manipulate factors affecting evidence quality and decision time or response urgency to more directly probe the processes underlying this structure.

Direct correspondence with the RPFs estimated in Chapter 1 should also be interpreted cautiously, as the surfaces here were constructed using nonparametric linear interpolation over the empirical accuracy-speed domain, whereas the earlier RPFs were estimated parametrically. This nonparametric approach minimizes assumptions about the form of a multidimensional relationship, but developing parametric implementations represents an important direction for future work. Such models could provide compact descriptions of surface geometry, facilitate comparisons across observers and conditions, and establish direct multidimensional analogues of existing parametric RPF methods.

3.5.2 Conclusion

Together, these findings demonstrate the value of characterizing confidence over a multidimensional behavioral domain. Extending the RPF framework from a relative function to a surface revealed that confidence depends jointly on accuracy and response speed, while their mapping onto confidence remains relatively stable across the visual field. More broadly, this approach provides a flexible framework

for characterizing multidimensional relationships between perception and metacognition and a new empirical target for theories of confidence.

General Conclusion

Through this dissertation, I have asked a deceptively simple question: when we look out into the world, do we know how well we see it?

Some of the limits of vision are obvious: we cannot read a page held far into the periphery or make out a detail too faint to see. Yet these limits blend seamlessly into ordinary visual experience. Perceptual ability changes dramatically from one location to another, yet we do not experience the visual world as a map of those differences. Somehow, from this uneven sensory landscape, we arrive at both a perceptual decision and a sense of how much to trust it.

Confidence neither reproduces perceptual performance nor floats free of it. Across the studies in this dissertation, confidence sometimes remained stable despite large variations in perception, and elsewhere changed where perceptual accuracy did not. Response speed carried information that accuracy left out. Sensory uncertainty mattered in ways that depended on the stimulus itself. There is no single transformation from perception to confidence.

These findings do not resolve whether peripheral visual experience is fundamentally rich or sparse, but they bear on the debate. Objective measurements make the limitations of peripheral vision impossible to deny, even when those limitations are not apparent from within the experience. Perhaps the question, then, is not only how much information is available in peripheral vision, but what our perceptual system tells us about the information that is missing. This dissertation has concerned the latter: not the contents of peripheral experience, but what observers know about the quality of their experience.

The question is therefore not simply whether metacognition is accurate. Knowing about one variation in our perception does not mean knowing about another. Nor is there necessarily one property of perceptual evidence that confidence ought to reproduce. Accuracy, speed, sensory uncertainty, spatial location, and the strength of the sensory signal each describe something different about the conditions under which a perceptual decision is made. What feels like a single judgment of confidence may therefore be the endpoint of many different sources of information. There is no single dimension to transform, either.

If different aspects of perception give rise to confidence in different ways, perhaps that diversity is part of the phenomenon we need to explain.

BIBLIOGRAPHY

Abrams, J., Nizam, A., and Carrasco, M. (2012). Isoeccentric locations are not equivalent: The extent of the vertical meridian asymmetry. *Vision Research*, 52(1):70–78.

Adler, W. T. and Ma, W. J. (2018). Comparing bayesian and non-bayesian accounts of human confidence reports. *PLoS Computational Biology*, 14(11):e1006572.

Aitchison, L., Bang, D., Bahrami, B., and Latham, P. E. (2015). Doubly bayesian analysis of confidence in perceptual decision-making. *PLoS computational biology*, 11(10):e1004519.

Altpeter, E., Mackeben, M., and Trauzettel-Klosinski, S. (2000). The importance of sustained attention for patients with maculopathies. *Vision Research*, 40(10-12):1539–1547.

Baldwin, A. S., Meese, T. S., and Baker, D. H. (2012). The attenuation surface for contrast sensitivity has the form of a witch's hat within the central visual field. *Journal of Vision*, 12(11):23–23.

Baranski, J. V. and Petrusic, W. M. (1994). The calibration and resolution of confidence in perceptual judgments. *Perception & Psychophysics*, 55(4):412–428.

Barbot, A., Xue, S., and Carrasco, M. (2021). Asymmetries in visual acuity around the visual field. *Journal of Vision*, 21(1):2–2.

Bates, D., Mächler, M., Bolker, B., and Walker, S. (2015). Fitting linear mixed-effects models using lme4. *Journal of Statistical Software*, 67(1):1–48.

Ben-Shachar, M. S., Lüdecke, D., and Makowski, D. (2020). effectsize: Estimation of effect size indices and standardized parameters. *Journal of Open Source Software*, 5(56):2815.

Benson, N. C., Kupers, E. R., Barbot, A., Carrasco, M., and Winawer, J. (2021). Cortical magnification in human visual cortex parallels task performance around the visual field. *Elife*, 10:e67685.

Boldt, A., de Gardelle, V., and Yeung, N. (2017). The impact of evidence reliability on sensitivity and bias in decision confidence. *Journal of Experimental Psychology: Human Perception and Performance*, 43(8):1520–1531.

Boldt, A., Sun, Y., and Desender, K. (2025). How disconfirmatory evidence shapes confidence in decision-making. *Communications Psychology*, 3(1):150.

Boundy-Singer, Z. M., Ziemba, C. M., and Goris, R. L. (2023). Confidence reflects a noisy decision reliability estimate. *Nature Human Behaviour*, 7(1):142–154.

Carrasco, M., Giordano, A. M., and McElree, B. (2004). Temporal performance fields: Visual and attentional factors. *Vision Research*, 44(12):1351–1365.

Carrasco, M., McElree, B., Denisova, K., and Giordano, A. M. (2003). Speed of visual processing increases with eccentricity. *Nature Neuroscience*, 6(7):699–700.

Carrasco, M., Talgar, C. P., and Cameron, E. L. (2001). Characterizing visual performance fields: Effects of transient covert attention, spatial frequency, eccentricity, task and set size. *Spatial Vision*, 15(1):61.

Carrasco, M., Williams, P. E., and Yeshurun, Y. (2002). Covert attention increases spatial resolution with or without masks: Support for signal enhancement. *Journal of Vision*, 2(6):4–4.

Christie, L. S. and Luce, R. D. (1956). Decision structure and time relations in simple choice behavior. *The bulletin of mathematical biophysics*, 18(2):89–112.

Clarke, F. R., Birdsall, T. G., and Tanner Jr, W. P. (1959). Two types of roc curves and definitions of parameters. *The Journal of the Acoustical Society of America*, 31(5):629–630.

Cleeremans, A., Timmermans, B., and Pasquali, A. (2007). Consciousness and metarepresentation: A computational sketch. *Neural Networks*, 20(9):1032–1039.

Corbett, J. E. and Carrasco, M. (2011). Visual performance fields: Frames of reference. *PLoS One*, 6(9):e24470.

Cortese, A., Amano, K., Koizumi, A., Kawato, M., and Lau, H. (2016). Multivoxel neurofeedback selectively modulates confidence without changing perceptual performance. *Nature Communications*, 7(1):13669.

Curcio, C. A. and Allen, K. A. (1990). Topography of ganglion cells in human retina. *Journal of Comparative Neurology*, 300(1):5–25.

Curcio, C. A., Sloan, K. R., Kalina, R. E., and Hendrickson, A. E. (1990). Human photoreceptor topography. *Journal of Comparative Neurology*, 292(4):497–523.

Denison, R. N., Adler, W. T., Carrasco, M., and Ma, W. J. (2018). Humans incorporate attention-dependent uncertainty into perceptual decisions and confidence. *Proceedings of the National Academy of Sciences*, 115(43):11090–11095.

Desender, K., Boldt, A., and Yeung, N. (2018). Subjective confidence predicts information seeking in decision making. *Psychological Science*, 29(5):761–778.

Eriksen, C. W. and St. James, J. D. (1986). Visual attention within and around the field of focal attention: A zoom lens model. *Perception & psychophysics*, 40(4):225–240.

Fetsch, C. R., Kiani, R., Newsome, W. T., and Shadlen, M. N. (2014). Effects of cortical microstimulation on confidence in a perceptual decision. *Neuron*, 83(4):797–804.

Fleming, S. M. (2024). Metacognition and confidence: A review and synthesis. *Annual Review of Psychology*, 75(1):241–268.

Fleming, S. M. and Daw, N. D. (2017). Self-evaluation of decision-making: A general bayesian framework for metacognitive computation. *Psychological Review*, 124(1):91.

Fleming, S. M., Huijgen, J., and Dolan, R. J. (2012). Prefrontal contributions to metacognition in perceptual decision making. *Journal of Neuroscience*, 32(18):6117–6125.

Fleming, S. M. and Lau, H. C. (2014). How to measure metacognition. *Frontiers in Human Neuroscience*, 8:443.

Fleming, S. M., Weil, R. S., Nagy, Z., Dolan, R. J., and Rees, G. (2010). Relating introspective accuracy to individual differences in brain structure. *Science*, 329(5998):1541–1543.

Fuller, S., Rodriguez, R. Z., and Carrasco, M. (2008). Apparent contrast differs across the vertical meridian: Visual and attentional factors. *Journal of Vision*, 8(1):16–16.

Fung, H., Shekhar, M., Xue, K., Rausch, M., and Rahnev, D. (2025). Similarities and differences in the effects of different stimulus manipulations on accuracy and confidence. *Consciousness and cognition*, 136:103942.

Galvin, S. J., Podd, J. V., Drga, V., and Whitmore, J. (2003). Type 2 tasks in the theory of signal detectability: Discrimination between correct and incorrect decisions. *Psychonomic Bulletin & Review*, 10:843–876.

Gold, J. I. and Shadlen, M. N. (2007). The neural basis of decision making. *Annual Review of Neuroscience*, 30(1):535–574.

Gorea, A. and Sagi, D. (2000). Failure to handle more than one internal representation in visual detection tasks. *Proceedings of the National Academy of Sciences*, 97(22):12380–12384.

Greenwood, J. A., Szinte, M., Sayim, B., and Cavanagh, P. (2017). Variations in crowding, saccadic precision, and spatial localization reveal the shared topology of spatial vision. *Proceedings of the National Academy of Sciences*, 114(17):E3573–E3582.

Hangya, B., Sanders, J. I., and Kepecs, A. (2016). A mathematical framework for statistical decision confidence. *Neural Computation*, 28(9):1840–1858.

Heitz, R. P. (2014). The speed-accuracy tradeoff: history, physiology, methodology, and behavior. *Frontiers in neuroscience*, 8:150.

Hellmann, S., Zehetleitner, M., and Rausch, M. (2023). Simultaneous modeling of choice, confidence, and response time in visual perception. *Psychological review*, 130(6):1521.

Hellmann, S., Zehetleitner, M., and Rausch, M. (2024). Confidence is influenced by evidence accumulation time in dynamical decision models. *Computational Brain & Behavior*, 7(3):287–313.

Henmon, V. A. C. (1911). The relation of the time of a judgment to its accuracy. *Psychological review*, 18(3):186.

Herce Castañón, S., Moran, R., Ding, J., Egner, T., Bang, D., and Summerfield, C. (2019). Human noise blindness drives suboptimal cognitive inference. *Nature Communications*, 10(1):1719.

Herregods, S., Le Denmat, P., Vermeylen, L., and Desender, K. (2025). Modeling speed–accuracy trade-offs in the stopping rule for confidence judgments. *Psychological Review*.

Himmelberg, M. M., Kurzawski, J. W., Benson, N. C., Pelli, D. G., Carrasco, M., and Winawer, J. (2021). Cross-dataset reproducibility of human retinotopic maps. *Neuroimage*, 244:118609.

Himmelberg, M. M., Kwak, Y., Carrasco, M., and Winawer, J. (2025). Unpacking the v1 map: Differential covariation of preferred spatial frequency and cortical magnification across spatial dimensions. *PLOS Computational Biology*, 21(10):1–27.

Himmelberg, M. M., Winawer, J., and Carrasco, M. (2022). Linking individual differences in human primary visual cortex to contrast sensitivity around the visual field. *Nature Communications*, 13(1):3309.

Himmelberg, M. M., Winawer, J., and Carrasco, M. (2023). Polar angle asymmetries in visual perception and neural architecture. *Trends in Neurosciences*, 46(6):445–458.

Jang, Y., Wallsten, T. S., and Huber, D. E. (2012). A stochastic detection and retrieval model for the study of metacognition. *Psychological Review*, 119(1):186.

Jigo, M., Tavdy, D., Himmelberg, M. M., and Carrasco, M. (2023). Cortical magnification eliminates differences in contrast sensitivity across but not around the visual field. *Elife*, 12:e84205.

Jovanovic, L. and Mamassian, P. (2019). When an event is perceived depends on where we attend. *i-Perception*, 10(3):2041669519858096.

Jovanovic, L. and Mamassian, P. (2020). Events are perceived earlier in peripheral vision. *Current Biology*, 30(21):R1299–R1300.

Kepecs, A. and Mainen, Z. F. (2012). A computational framework for the study of confidence in humans and animals. *Philosophical Transactions of the Royal Society B: Biological Sciences*, 367(1594):1322.

Kiani, R., Corthell, L., and Shadlen, M. N. (2014). Choice certainty is informed by both evidence and decision time. *Neuron*, 84(6):1329–1342.

Kiani, R. and Shadlen, M. N. (2009). Representation of confidence associated with a decision by neurons in the parietal cortex. *Science*, 324(5928):759–764.

Ko, Y. H., Feuerriegel, D., Turner, W., Overhoff, H., Niessen, E., Stahl, J., Hester, R., Fink, G. R., Weiss, P. H., and Bode, S. (2022). Divergent effects of absolute evidence magnitude on decision accuracy and confidence in perceptual judgements. *Cognition*, 225:105125.

Koizumi, A., Maniscalco, B., and Lau, H. (2015). Does perceptual confidence facilitate cognitive control? *Attention, Perception, & Psychophysics*, 77:1295–1306.

Kupers, E. R., Benson, N. C., Carrasco, M., and Winawer, J. (2022). Asymmetries around the visual field: From retina to cortex to behavior. *PLoS computational biology*, 18(1):e1009771.

Kupers, E. R., Carrasco, M., and Winawer, J. (2019). Modeling visual performance differences 'around'the visual field: A computational observer approach. *PLoS computational biology*, 15(5):e1007063.

Kuznetsova, A., Brockhoff, P. B., and Christensen, R. H. B. (2017). lmerTest package: Tests in linear mixed effects models. *Journal of Statistical Software*, 82(13):1–26.

Lau, H. C. and Passingham, R. E. (2006). Relative blindsight in normal observers and the neural correlate of visual consciousness. *Proceedings of the National Academy of Sciences*, 103(49):18763–18768.

Lenth, R. V. and Piaskowski, J. (2026). *emmeans: Estimated Marginal Means, aka Least-Squares Means*. R package version 2.0.3.

Li, M. K., Lau, H., and Odegaard, B. (2018). An investigation of detection biases in the unattended periphery during simulated driving. *Attention, Perception, & Psychophysics*, 80:1325–1332.

Liu, T., Heeger, D. J., and Carrasco, M. (2006). Neural correlates of the visual vertical meridian asymmetry. *Journal of Vision*, 6(11):12–12.

Mackeben, M. (1999). Sustained focal attention and peripheral letter recognition. *Spatial Vision*, 12(1):51–72.

Mamassian, P. (2016). Visual confidence. *Annual Review of Vision Science*, 2:459–481.

Maniscalco, B., Graham Castaneda, O., Odegaard, B., Morales, J., Rajananda, S., Denison, R. N., and Peters, M. A. (2026). The relative psychometric function: a general analysis framework for relating psychological processes. *Psychological Review*.

Maniscalco, B. and Lau, H. (2012). A signal detection theoretic approach for estimating metacognitive sensitivity from confidence ratings. *Consciousness and Cognition*, 21(1):422–430.

Maniscalco, B. and Lau, H. (2014). Signal detection theory analysis of type 1 and type 2 data: meta-d, response-specific meta-d, and the unequal variance sdt model. In *The cognitive neuroscience of metacognition*, pages 25–66. Springer.

Maniscalco, B. and Lau, H. (2016). The signal processing architecture underlying subjective reports of sensory awareness. *Neuroscience of Consciousness*, 2016(1):niw002.

Maniscalco, B., Odegaard, B., Grimaldi, P., Cho, S. H., Basso, M. A., Lau, H., and Peters, M. A. (2021). Tuned inhibition in perceptual decision-making circuits can explain seemingly suboptimal confidence behavior. *PLoS Computational Biology*, 17(3):e1008779.

Maniscalco, B., Peters, M. A., and Lau, H. (2016). Heuristic use of perceptual evidence leads to dissociation between performance and metacognitive sensitivity. *Attention, Perception, & Psychophysics*, 78:923–937.

Miyoshi, K. and Lau, H. (2020). A decision-congruent heuristic gives superior metacognitive sensitivity under realistic variance assumptions. *Psychological Review*, 127(5):655.

Miyoshi, K. and Sakamoto, Y. (2025). Early sensory evidence shapes multichoice confidence bias: A registered report. *Journal of Experimental Psychology: General*.

Miyoshi, K., Webb, T., Rahnev, D., and Lau, H. (2024). Confidence and metacognition. *Reference Module in Neuroscience and Biobehavioral Psychology. Elsevier*, 10.

Morales, J., Odegaard, B., and Maniscalco, B. (2022). 10 the neural substrates of conscious perception without performance confounds. *Neuroscience and Philosophy*, page 285.

Morales, J., Solovey, G., Maniscalco, B., Rahnev, D., de Lange, F. P., and Lau, H. (2015). Low attention impairs optimal incorporation of prior knowledge in perceptual decisions. *Attention, Perception, & Psychophysics*, 77:2021–2036.

Moran, R., Teodorescu, A. R., and Usher, M. (2015). Post choice information integration as a causal determinant of confidence: Novel data and a computational account. *Cognitive Psychology*, 78:99–147.

Morey, R. D. and Rouder, J. N. (2026). *BayesFactor: Computation of Bayes Factors for Common Designs*. R package version 0.9.12-4.8.

Odegaard, B., Chang, M. Y., Lau, H., and Cheung, S.-H. (2018a). Inflation versus filling-in: why we feel we see more than we actually do in peripheral vision. *Philosophical Transactions of the Royal Society B: Biological Sciences*, 373(1755):20170345.

Odegaard, B., Grimaldi, P., Cho, S. H., Peters, M. A., Lau, H., and Basso, M. A. (2018b). Superior colliculus neuronal ensemble activity signals optimal rather than subjective confidence. *Proceedings of the National Academy of Sciences*, 115(7):E1588–E1597.

Okubo, L., Miyoshi, K., Yokosawa, K., and Nishida, S. (2026). Inattentional noise leads to subjective color uniformity across the visual field. *Cognition*, 266:106293.

Okubo, L. and Yokosawa, K. (2023). Attentional allocation and the pan-field color illusion. *Journal of Vision*, 23(3):13–13.

Pereira, M., Faivre, N., Iturrate, I., Wirthlin, M., Serafini, L., Martin, S., Desvachez, A., Blanke, O., Van De Ville, D., and Millán, J. d. R. (2020). Disentangling the origins of confidence in speeded perceptual judgments through multimodal imaging. *Proceedings of the National Academy of Sciences*, 117(15):8382–8390.

Peters, M. A. (2022). Towards characterizing the canonical computations generating phenomenal experience. *Neuroscience & Biobehavioral Reviews*, page 104903.

Peters, M. A., Fesi, J., Amendi, N., Knotts, J. D., Lau, H., and Ro, T. (2017a). Transcranial magnetic stimulation to visual cortex induces suboptimal introspection. *Cortex*, 93:119–132.

Peters, M. A., Thesen, T., Ko, Y. D., Maniscalco, B., Carlson, C., Davidson, M., Doyle, W., Kuzniecky, R., Devinsky, O., Halgren, E., and Lau, H. (2017b). Perceptual confidence neglects decision-incongruent evidence in the brain. *Nature Human Behaviour*, 1(7):0139.

Pleskac, T. J. and Busemeyer, J. R. (2010). Two-stage dynamic signal detection: a theory of choice, decision time, and confidence. *Psychological Review*, 117(3):864.

Prins, N. and Kingdom, F. A. (2018). Applying the model-comparison approach to test specific research hypotheses in psychophysical research using the palamedes toolbox. *Frontiers in psychology*, 9:1250.

Pruitt, J., Knotts, J., and Odegaard, B. (2024). Consistent metacognitive efficiency and variable response biases in peripheral vision. *Journal of Vision*, 24(8):4–4.

Rahnev, D. (2025). A comprehensive assessment of current methods for measuring metacognition. *Nature Communications*, 16(1):701.

Rahnev, D. (2026). Confidence-accuracy dissociations in perceptual decision making. *Vision Research*, 244:108831.

Rahnev, D. A. (2021). Visual metacognition: Measures, models, and neural correlates. *American Psychologist*, 76(9):1445.

Rahnev, D. A. and Fleming, S. M. (2019). How experimental procedures influence estimates of metacognitive ability. *Neuroscience of Consciousness*, 2019(1):niz009.

Rahnev, D. A., Maniscalco, B., Graves, T., Huang, E., De Lange, F. P., and Lau, H. (2011). Attention induces conservative subjective biases in visual perception. *Nature Neuroscience*, 14(12):1513–1515.

Rahnev, D. A., Maniscalco, B., Luber, B., Lau, H., and Lisanby, S. H. (2012). Direct injection of noise to the visual cortex decreases accuracy but increases decision confidence. *Journal of Neurophysiology*, 107(6):1556–1563.

Rajananda, S., Peters, M. A., Lau, H., and Odegaard, B. (2017). Subjective inflation of color saturation in the periphery under temporal overload. *BioRxiv*, page 227074.

Rausch, M., Hellmann, S., and Zehetleitner, M. (2018). Confidence in masked orientation judgments is informed by both evidence and visibility. *Attention, Perception, & Psychophysics*, 80:134–154.

Rausch, M., Hellmann, S., and Zehetleitner, M. (2021). Modelling visibility judgments using models of decision confidence. *Attention, Perception, & Psychophysics*, 83(8):3311–3336.

Reynolds, J. H. and Heeger, D. J. (2009). The normalization model of attention. *Neuron*, 61(2):168–185.

Rijsdijk, J., Kroon, J., and Van der Wildt, G. (1980). Contrast sensitivity as a function of position on the retina. *Vision Research*, 20(3):235–241.

Rong, Y. and Peters, M. A. (2023). Toward 'computational-rationality'approaches to arbitrating models of cognition: A case study using perceptual metacognition. *Open Mind*, 7:652–674.

Rounis, E., Maniscalco, B., Rothwell, J. C., Passingham, R. E., and Lau, H. (2010). Theta-burst transcranial magnetic stimulation to the prefrontal cortex impairs metacognitive visual awareness. *Cognitive Neuroscience*, 1(3):165–175.

Samaha, J., Barrett, J. J., Sheldon, A. D., LaRocque, J. J., and Postle, B. R. (2016). Dissociating perceptual confidence from discrimination accuracy reveals no influence of metacognitive awareness on working memory. *Frontiers in Psychology*, 7:851.

Samaha, J. and Denison, R. (2022). The positive evidence bias in perceptual confidence is unlikely post-decisional. *Neuroscience of Consciousness*, 2022(1):niac010.

Samaha, J., Iemi, L., and Postle, B. R. (2017). Prestimulus alpha-band power biases visual discrimination confidence, but not accuracy. *Consciousness and Cognition*, 54:47–55.

Samaha, J., Switzky, M., and Postle, B. R. (2019). Confidence boosts serial dependence in orientation estimation. *Journal of Vision*, 19(4):25–25.

Schmolesky, M. T., Wang, Y., Hanes, D. P., Thompson, K. G., Leutgeb, S., Schall, J. D., and Leventhal, A. G. (1998). Signal timing across the macaque visual system. *Journal of Neurophysiology*, 79(6):3272–3278.

Shadlen, M. N. and Kiani, R. (2013). Decision making as a window on cognition. *Neuron*, 80(3):791–806.

Sharvashidze, N., Toscani, M., and Valsecchi, M. (2025). Peripheral overconfidence in a scene categorization task. *Journal of Vision*, 25(10):2–2.

Shekhar, M. and Rahnev, D. (2021). The nature of metacognitive inefficiency in perceptual decision making. *Psychological review*, 128(1):45.

Shekhar, M. and Rahnev, D. (2023). How do humans give confidence? a comprehensive comparison of process models of perceptual metacognition. *Journal of Experimental Psychology: General*.

Shen, A. and Peters, M. (2026). Stimulus properties and visual field location interact to drive performance-independent perceptual confidence.

Singmann, H., Bolker, B., Westfall, J., Aust, F., and Ben-Shachar, M. S. (2025). *afex: Analysis of Factorial Experiments*. R package version 1.5-1.

Solovey, G., Graney, G. G., and Lau, H. (2015). A decisional account of subjective inflation of visual perception at the periphery. *Attention, Perception, & Psychophysics*, 77:258–271.

Strasburger, H., Rentschler, I., and Jüttner, M. (2011). Peripheral vision and pattern recognition: A review. *Journal of Vision*, 11(5):1–82.

Talgar, C. P. and Carrasco, M. (2002). Vertical meridian asymmetry in spatial resolution: Visual and attentional factors. *Psychonomic Bulletin & Review*, 9:714–722.

Tian, K. J., Maniscalco, B., Epstein, M. L., Shen, A., Castaneda, O. G., Kurosawa, T., Motzer, J. A., Olsson, E., Russell, E. E., Walsh, M. E., et al. (2025). Attention robustly dissociates objective performance and subjective visibility reports. *bioRxiv*, pages 2025–07.

Toscani, M., Mamassian, P., and Valsecchi, M. (2021). Underconfidence in peripheral vision. *Journal of Vision*, 21(6):2–2.

Upadhyayula, A., Phillips, I., and Flombaum, J. (2023). Eccentricity advances arrival to visual perception. *Journal of Experimental Psychology: General*.

Vandenbroucke, A. R., Sligte, I. G., Barrett, A. B., Seth, A. K., Fahrenfort, J. J., and Lamme, V. A. (2014). Accurate metacognition for visual sensory memory representations. *Psychological Science*, 25(4):861–873.

Watson, A. B. (2014). A formula for human retinal ganglion cell receptive field density as a function of visual field location. *Journal of Vision*, 14(7):15–15.

Weidemann, C. T. and Kahana, M. J. (2016). Assessing recognition memory using confidence ratings and response times. *Royal Society open science*, 3(4):150670.

Wickelgren, W. A. (1977). Speed-accuracy tradeoff and information processing dynamics. *Acta psychologica*, 41(1):67–85.

Winter, C. J. and Peters, M. A. (2022). Variance misperception under skewed empirical noise statistics explains overconfidence in the visual periphery. *Attention, Perception, & Psychophysics*, 84(1):161–178.

Xue, S., Barbot, A., Abrams, J., Chen, Q., and Carrasco, M. (2026a). Distinct system-level computations underlie perceptual variation across the visual field. *Proceedings of the National Academy of Sciences*, 123(17):e2533752123.

Xue, S., Landy, M., and Carrasco, M. (2026b). Featural representation and internal noise around the visual field. *bioRxiv*.

Yeung, N. and Summerfield, C. (2012). Metacognition in human decision-making: confidence and error monitoring. *Philosophical Transactions of the Royal Society B: Biological Sciences*, 367(1594):1310–1321.

Zylberberg, A., Barttfeld, P., and Sigman, M. (2012). The construction of confidence in a perceptual decision. *Frontiers in Integrative neuroscience*, 6:79.

Zylberberg, A., Fetsch, C. R., and Shadlen, M. N. (2016). The influence of evidence volatility on choice, reaction time and confidence in a perceptual decision. *Elife*, 5:e17688.

Zylberberg, A., Roelfsema, P. R., and Sigman, M. (2014). Variance misperception explains illusions of confidence in simple perceptual decisions. *Consciousness and Cognition*, 27:246–253.